NASA Technical Memorandum 84316

Mathematical Model of the SH-3G Helicopter

James D. Phillips

December 1982

National Aeronautics and
Space Administration

NASA Technical Memorandum 84316

Mathematical Model of the SH-3G Helicopter

James D. Phillips
Ames Research Center, Moffett Field, California

National Aeronautics and
Space Administration

Ames Research Center
Moffett Field, California 94035

TABLE OF CONTENTS

SUMMARY

A mathematical model of the Sikorsky SH-3G helicopter based on classical nonlinear, "quasi-steady" rotor theory has been developed at NASA Ames Research Center. The model has been validated statically and dynamically by comparison with Navy flight-test data. The model incorporates ad hoc revisions which address the ideal assumptions of classical rotor theory and improve the static trim characteristics to provide a more realistic simulation, while retaining the simplicity of the classical model.

INTRODUCTION

The Guidance and Navigation Branch at Ames Research Center is conducting research to improve helicopter IFR operations at remote sites and at high-density traffic areas. Much of the research is accomplished using a Sikorsky SH-3G helicopter (see fig. 1) to evaluate advanced guidance and navigation concepts. Prior to flight test, new concepts are developed on an off-line simulation or using a real-time piloted simulation. A requirement, then, exists to develop and validate an off-line math model of the SH-3G which can be adapted for real-time simulation.

In recent years, NASA has developed several simulations of Sikorsky aircraft. In 1979, J. D. Shaughnessy of Langley Research Center developed a math model of the Sikorsky CH-54 helicopter for sling-load research (ref. 1). The rotor models used were based largely on an NACA report by F. J. Bailey (ref. 2), who related rotor performance to only three varying parameters: the inflow ratio, the tip-speed ratio, and the rotor pitch. However, Bailey assumed uniform downwash which leads to underestimating the induced power by approximately 11% in hover, and 17% in high forward flight (ref. 3, p. 140). In 1980, Sturgeon and Phillips (NASA Ames) modified Shaughnessy's model to simulate the Sikorsky CH-53 (ref. 4).

This paper documents a mathematical model of the SH-3G helicopter which was developed by modifying and adding to the existing CH-53 helicopter math model at Ames, and validated by matching flight data. The present model differs from the CH-54 and CH-53 models in that actual static performance as measured in flight test (ref. 5) is more closely matched by addressing the assumptions of uniform downwash, two-dimensional, blade lift curve slope, and fuselage flat-plate area as measured in the wind tunnel. In addition, the fuselage aerodynamics, equations of motion, and engine model are simplified. An improved trimming algorithm has also been implemented.

Like the CH-53 math model, the SH-3G math model calculates nonlinear rotor aerodynamics based on the "quasi-steady" assumption, i.e., there are no unsteady aerodynamic effects between time steps. The fuselage aerodynamics have been linearized as much as possible and the engine and associated governor are modeled by a simple transfer function between the main-rotor rpm deviation from nominal and the engine torque.

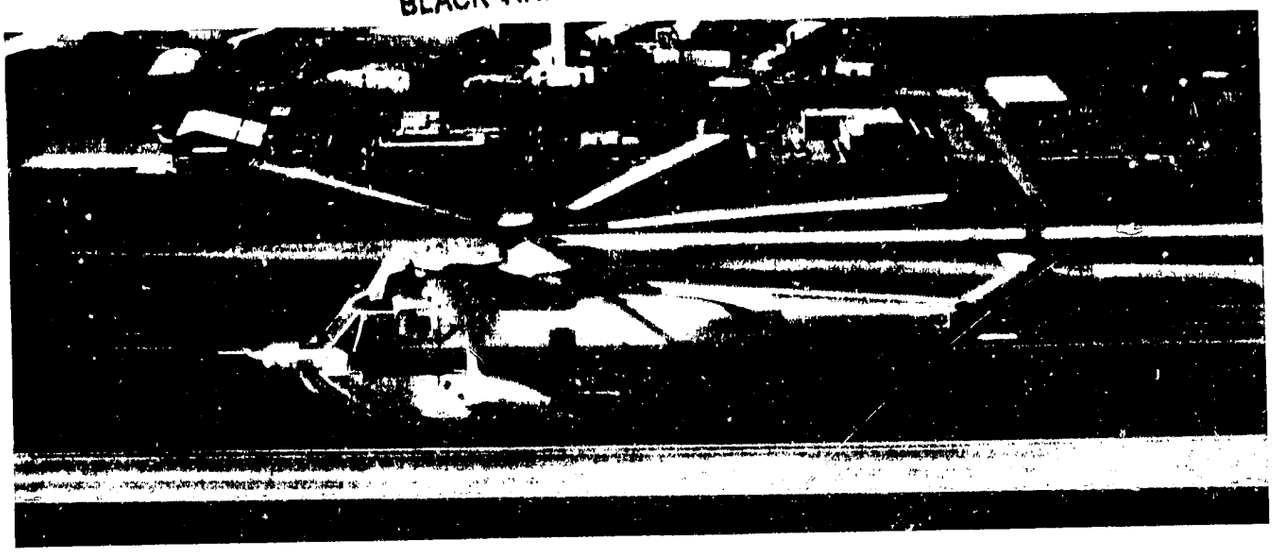

Figure 1.- NASA SH-3G research helicopter.

MATHEMATICAL MODEL

The SH-3G math model consists of eight submodels: the equations of motion, the atmospheric model, the wind, the fuselage aerodynamics, the main rotor, the tail rotor, the engine, and the control system and rigging. A description of the coordinate systems used throughout, a general description of all the submodels, and a detailed description of each submodel follow.

Coordinate Systems

1. Earth axes, subscript e: Origin fixed on the earth's surface, x axis pointing north, y axis pointing east, and z axis pointing down into the earth. This coordinate system rotates with the earth with the z axis always pointing toward the earth's center.

2. Path axes, subscript p: Origin at the center of gravity of the helicopter, x axis pointing along the earth relative velocity vector, y axis pointing perpendicular to the right of the earth relative velocity vector and parallel to the ground, z axis pointing down and perpendicular to the earth relative velocity vector (see fig. 2).

3. Body axes, subscript b: Origin at the center of gravity of the helicopter, x axis pointing out the nose of the helicopter, y axis pointing to the right perpendicular to the plane of symmetry, and z axis down in the plane of symmetry (see fig. 3).

4. Shaft axes, subscript s: Origin at the rotor hub, x axis rotated about the y body axis through the longitudinal shaft tilt angle, θ_s, y axis rotated about the new shaft x axis through the lateral shaft tilt angle, ϕ_s, and z axis down and parallel to the shaft (see fig. 4).

5. Control axes, subscript c: Origin at the rotor hub, x axis pointing toward the relative wind parallel to the swashplate, y axis pointing to the right parallel to the swashplate (perpendicular to the relative wind), and z axis down and perpendicular to the swashplate (see fig. 5).

6. Wind axes, subscript w: Origin at the center of gravity of the helicopter, x axis pointing into the relative wind, y axis rotated about the z axis by the sideslip angle, β, and z axis rotated about the y wind axis by the angle of attack, α (see fig. 6).

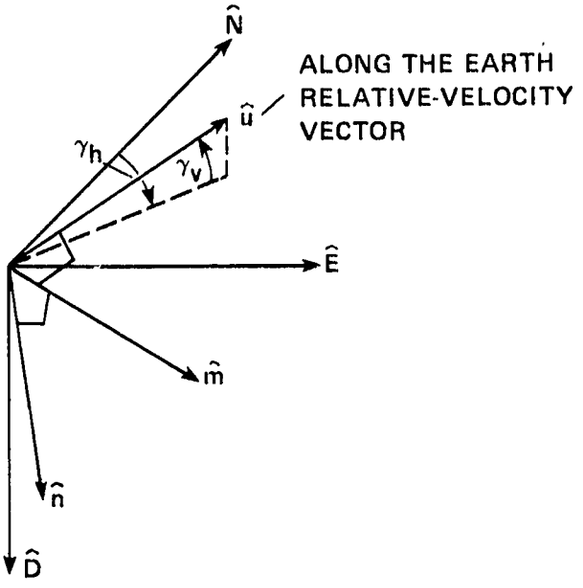

Figure 2.- Path axes.

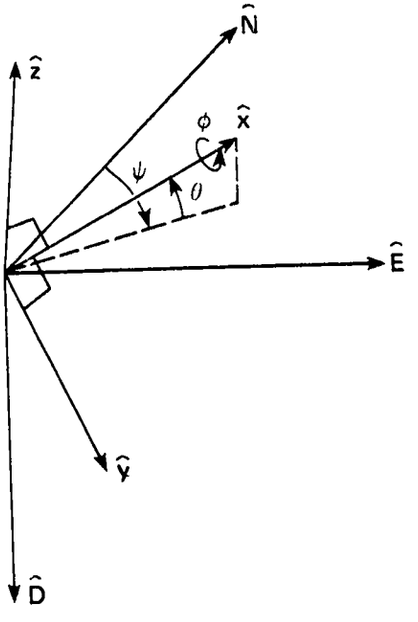

Figure 3.- Body axes.

General Model Description

The SH-3G helicopter simulation contains the following submodels:

1. Equations of motion: This submodel calculates the position, velocity, acceleration, attitude, angular velocity, and angular acceleration from the forces and moments provided from other submodels.

2. Atmospheric model: Atmosphere pressure, temperature, density, and dynamic pressure are calculated from the 1962 standard atmosphere.

3. Wind model: Turbulence and steady-wind components are generated in this submodel. The random turbulence conforms to the Dryden spectral model.

4. Fuselage aerodynamics model: The fuselage aerodynamics model determines the lift, drag, and side forces, as well as the pitching, rolling, and yawing moments as functions of the fuselage angle of attack, the fuselage sideslip angle, and the dynamic pressure. In the interest of simplicity, the functions are all linear or polynomial functions of sinusoids.

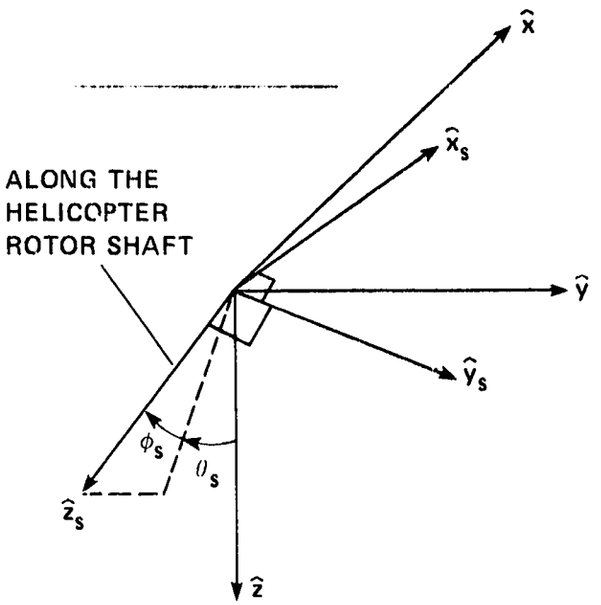

Figure 4.- Shaft axes.

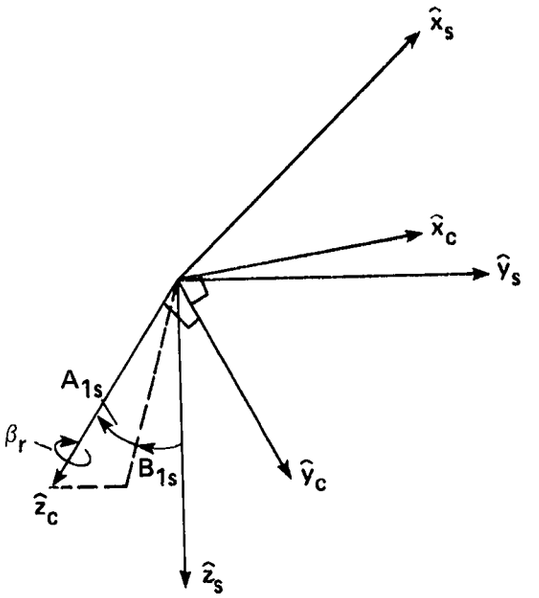

Figure 5.- Control axes.

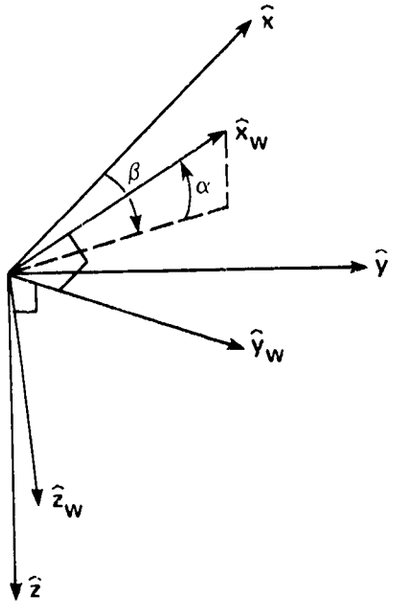

Figure 6.- Wind axes.

5. Main-rotor model: This submodel determines the nonlinear thrust, drag, side forces, and hub moments assuming quasi-steady dynamics. The model accounts for variable inflow ratio, variable rotor speed, blade twist, tip loss, blade coning, blade flapping, flapping-hinge offset, nonuniform blade loading, and profile drag due to spanwise flow.

6. Tail rotor model: This submodel is the same as the main-rotor model except that a δ_3 hinge (detailed description in a later section) is accounted for, there are no commanded cyclic-flapping angles, and initialization of the inflow ratio requires a more complicated iterative process.

7. Engine model: The engine is modeled as a torque-producing device acting on a pure inertia. The engine governor is a proportional plus integral controller.

8. Control system and rigging model: Transfer functions between the pilot's cyclic stick, collective stick, and rudder pedals to the main-rotor collective pitch, cyclic swashplate angles, and tail rotor collective pitch are modeled. The SH-3G ASE (automatic stabilization equipment) and barometric altitude hold are modeled.

The relationships between the various submodels are illustrated in figure 7.

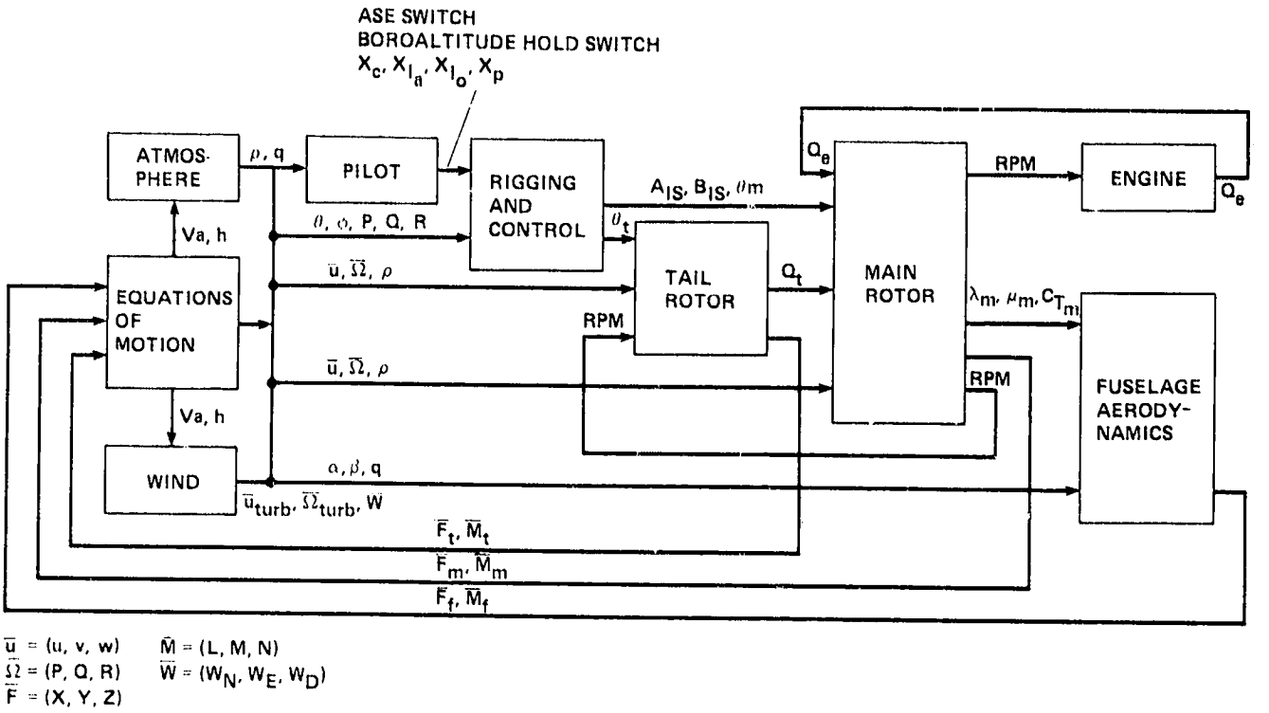

Figure 7.- SH-3G math model block diagram.

Equations of Motion

The SH-3G equations of motion are a simplified version of SMART, a standard subroutine for simulation at Ames and documented in reference 6. SMART converts forces and moments from body axes to earth axes, integrates in earth coordinates to determine the earth relative velocity and position and converts the velocities back to body axes.

The SH-3G version of SMART deletes the small earth Coriolis effects and uses equations for the standard atmosphere instead of a table. A more convenient initialization has also been implemented (see appendix A).

The body-axis forces generated in the fuselage aerodynamics model, the main-rotor model, and the tail-rotor model are summed to produce the total body-axis forces acting on the helicopter.

The total body-axis forces are related to the earth-axis forces by the familiar Euler angle rotations:

$$\begin{pmatrix} F_x \\ F_y \\ F_z \end{pmatrix} = T_\phi T_\theta T_\psi \begin{pmatrix} F_N \\ F_E \\ F_D \end{pmatrix} \tag{1}$$

where:

$$T_\phi = \begin{vmatrix} 1 & 0 & 0 \\ 0 & C\phi & S\phi \\ 0 & -S\phi & C\phi \end{vmatrix} \quad ; \quad T_\theta = \begin{vmatrix} C\theta & 0 & -S\theta \\ 0 & 1 & 0 \\ S\theta & 0 & C\theta \end{vmatrix} \quad ; \quad T_\psi = \begin{vmatrix} C\psi & S\psi & 0 \\ -S\psi & C\psi & 0 \\ 0 & 0 & 1 \end{vmatrix}$$

The trigonometric functions "sine" and "cosine" will be abbreviated "S" and "C" throughout this paper.

Solving for the earth relative forces:

$$\begin{pmatrix} F_N \\ F_E \\ F_D \end{pmatrix} = \begin{vmatrix} C\theta C\psi & S\phi S\theta C\psi - C\phi S\psi & C\phi S\theta C\psi + S\phi S\psi \\ C\theta S\psi & S\phi S\theta S\psi + C\phi C\psi & C\phi S\theta S\psi - S\phi C\psi \\ -S\theta & S\phi C\theta & C\phi C\theta \end{vmatrix} \times \begin{pmatrix} F_x \\ F_y \\ F_z \end{pmatrix} \tag{2}$$

If we neglect the earth Coriolis accelerations, but keep the earth centripetal accelerations, we find the earth's relative accelerations to be:

$$\begin{pmatrix} \dot{V}_N \\ \dot{V}_E \\ \dot{V}_D \end{pmatrix} = \frac{1}{m} \begin{pmatrix} F_N \\ F_E \\ F_D + F_G \end{pmatrix} - \begin{pmatrix} R_e \omega_e^2 \, C(LAT) S(LAT) \\ 0 \\ R_e \omega_e^2 \, C^2(LAT) \end{pmatrix} \tag{3}$$

where F_G is the gravitational force equal to the weight of the aircraft, m is the mass of the aircraft, R_e is the radius of the earth, and ω_e is the rate of angular rotation of the earth. The aircraft velocity magnitude relative to the earth has been neglected compared to the inertial velocity due to the earth's rotation.

The earth relative velocities are found by integrating the earth relative accelerations. A second-order Adams-Bashford predictor algorithm for integrating is used (as in ref. 6) yielding:

$$\begin{pmatrix} V_N \\ V_E \\ V_D \end{pmatrix}_{n+1} = \begin{pmatrix} V_N \\ V_E \\ V_D \end{pmatrix}_n + \left[3 \times \begin{pmatrix} \dot{V}_N \\ \dot{V}_E \\ \dot{V}_D \end{pmatrix}_n - \begin{pmatrix} \dot{V}_N \\ \dot{V}_E \\ \dot{V}_D \end{pmatrix}_{n-1} \right] \times \frac{DT}{2} \tag{4}$$

where DT is the integration time step, n is the present value, (n-1) is the previous value, and (n+1) is the next value.

The flightpath angles can now be found from their definitions:

$$\left.\begin{aligned} \gamma_V &= \arcsin\left(\frac{-V_D}{V}\right); \quad -\pi < \gamma_V \leq \pi; \quad V > 0 \\ \gamma_h &= \arctan\left(\frac{V_E}{V_N}\right); \quad -\frac{\pi}{2} < \gamma_h \leq \frac{\pi}{2}; \quad |V_N| > 0 \end{aligned}\right\} \tag{5}$$

where V is the magnitude of the earth relative velocity vector. By transforming the earth relative velocity vector to spherical coordinates, the latitude and longitude rates become:

$$\begin{aligned} \dot{LON} &= V_N/R_e \\ \dot{LAT} &= V_E/[R_e \times C(LAT)] \end{aligned} \tag{6}$$

Earth location is now found by numerical integration using a modified Euler method:

$$\begin{pmatrix} LON \\ LAT \\ ALT \end{pmatrix}_{n+1} = \begin{pmatrix} LON \\ LAT \\ ALT \end{pmatrix}_n + \left[\begin{pmatrix} \dot{LON} \\ \dot{LAT} \\ -\dot{V}_D \end{pmatrix}_n + \begin{pmatrix} \dot{LON} \\ \dot{LAT} \\ -\dot{V}_D \end{pmatrix}_{n-1} \right] \times \frac{DT}{2} \tag{7}$$

where ALT is the altitude above sea level.

The velocity with respect to the air in earth coordinates can be calculated from the vector equation:

$$\begin{pmatrix} V_{a_N} \\ V_{a_E} \\ V_{a_D} \end{pmatrix} = \begin{pmatrix} V_N \\ V_E \\ V_D \end{pmatrix} - \begin{pmatrix} W_N \\ W_E \\ W_D \end{pmatrix} \tag{8}$$

To transform to body coordinates, use the same Euler transformation as in equation (1):

$$\begin{pmatrix} U_b \\ V_b \\ W_b \end{pmatrix} = T_\phi T_\theta T_\psi \begin{pmatrix} V_{a_N} \\ V_{a_E} \\ V_{a_D} \end{pmatrix} \tag{9}$$

The angle of attack, α, and sideslip angle, β, can now be found from their definitions:

$$\left.\begin{aligned} \alpha &= \arctan\left(\frac{W_b}{U_b}\right); && \frac{-\pi}{2} < \alpha \leq \frac{\pi}{2} \\ \beta &= \arcsin\left[\frac{V_b}{V_a \ \mathrm{sign}(U_b)}\right]; && -\pi < \beta \leq \pi \end{aligned}\right\} \tag{10}$$

where $V_a = \sqrt{U_b^2 + V_b^2 + W_b^2}$, the magnitude of the air velocity and $|U_b| \neq 0$.

If the x-z plane is a plane of symmetry, the body-axis angular accelerations (from ref. 6) are:

$$\begin{pmatrix} \dot{P} \\ \dot{Q} \\ \dot{R} \end{pmatrix} = \begin{bmatrix} (C_1R + C_2P)Q \\ C_5RP + C_6(R^2 - P^2) \\ (C_8P + C_9R)Q \end{bmatrix} + \begin{bmatrix} C_3 & 0 & C_4 \\ 0 & C_7 & 0 \\ C_4 & 0 & C_{10} \end{bmatrix} \begin{pmatrix} L \\ M \\ N \end{pmatrix} \tag{11}$$

where L, M, and N are the total body axis moments generated by the rotor models and the fuselage aerodynamics and $C_1 \ldots C_{10}$ are inertial coefficients as follows:

$$\left.\begin{aligned} C_0 &= (I_{xx}I_{zz} - I_{xz}^2)^{-1} \\ C_1 &= C_0[(I_{yy} - I_{zz})I_{zz} - I_{xz}^2] \\ C_2 &= C_0I_{xz}(I_{xx} - I_{yy} + I_{zz}) \\ C_3 &= C_0I_{zz} \\ C_4 &= C_0I_{xz} \\ C_5 &= C_7(I_{zz} - I_{xx}) \\ C_6 &= C_7I_{xz} \\ C_7 &= I_{yy}^{-1} \\ C_8 &= C_0[(I_{xx} - I_{yy})I_{xx} + I_{xz}^2] \\ C_9 &= C_0I_{xz}(I_{yy} - I_{zz} - I_{xx}) \\ C_{10} &= C_0I_{xx} \end{aligned}\right\} \tag{12}$$

where I_{xx}, I_{yy}, I_{zz}, and I_{xz} are body axis moments of inertia.

Integrating the body angular accelerations using the second-order Adams-Bashford predictor algorithm yields the body-axis angular velocities:

$$\begin{pmatrix} P \\ Q \\ R \end{pmatrix}_{n+1} = \begin{pmatrix} P \\ Q \\ R \end{pmatrix}_{n} + \left[3 \times \begin{pmatrix} \dot{P} \\ \dot{Q} \\ \dot{R} \end{pmatrix}_{n} - \begin{pmatrix} \dot{P} \\ \dot{Q} \\ \dot{R} \end{pmatrix}_{n-1} \right] \times \frac{DT}{2} \tag{13}$$

The body axis acceleration vector is (see ref. 6):

$$\begin{pmatrix} \dot{U}_b \\ \dot{V}_b \\ \dot{W}_b \end{pmatrix} = \begin{pmatrix} 0 & -R & Q \\ R & 0 & -P \\ -Q & P & 0 \end{pmatrix} \begin{pmatrix} U_b \\ V_b \\ W_b \end{pmatrix} + T_\phi T_\theta T_\psi \begin{pmatrix} \dot{V}_N \\ \dot{V}_E \\ \dot{V}_D \end{pmatrix} \tag{14}$$

Neglecting the earth's angular velocity (7.2722*E-5 rad/sec), the Euler angular accelerations are:

$$\begin{pmatrix} \dot{\psi} \\ \dot{\theta} \\ \dot{\phi} \end{pmatrix} = \begin{pmatrix} (Q\ S\phi + R\ C\phi)/C\theta \\ Q\ C\phi - R\ S\phi \\ P + \dot{\psi}\ S\theta \end{pmatrix} \tag{15}$$

Integrating the Euler angular accelerations using the modified Euler algorithm:

$$\begin{pmatrix} \psi \\ \theta \\ \phi \end{pmatrix}_{n+1} = \begin{pmatrix} \psi \\ \theta \\ \phi \end{pmatrix}_{n} + \left[\begin{pmatrix} \dot{\psi} \\ \dot{\theta} \\ \dot{\phi} \end{pmatrix}_{n} + \begin{pmatrix} \dot{\psi} \\ \dot{\theta} \\ \dot{\phi} \end{pmatrix}_{n-1} \right] \times \frac{DT}{2} \tag{16}$$

Atmospheric Model

The pressure, temperature, and density of the atmosphere have important effects on the aerodynamics of any aircraft.

Since helicopters operate well below the speed of sound, conditions can be assumed subsonic. Most helicopters also operate in the troposphere (below 36,089 ft in the 1962 standard atmosphere) so for this case the atmosphere can be modeled by just two equations:

$$\left.\begin{aligned} T_{a_r} &= 1 - 6.875\ E\text{-}6 \times ALT \\ P_{a_r} &= T_{a_r}^{5.256} \end{aligned}\right\} \tag{17}$$

where T_{a_r} and P_{a_r} are the temperature and pressure ratios relative to standard sea-level values and ALT is the altitude above see level in feet.

For a diatomic gas such as air, the total temperature and pressure ratios are given by:

$$\left.\begin{aligned} T_r &= 1 + 0.2\ M^2 \\ P_r &= T_r^{3.5} \end{aligned}\right\} \tag{18}$$

where M is the Mach number.

The ambient conditions are now found as:

$$\left.\begin{aligned} T &= \Delta T + T_{a_r} * T_{std} \\ P &= P_{a_r} * P_{std} \\ \rho &= P/(T * 3088.8) \quad (P \text{ in psf, } T \text{ in Kelvin}) \\ V_{sound} &= 65.76\ \sqrt{T} \qquad (T \text{ in Kelvin}) \end{aligned}\right\} \tag{19}$$

where T_{std} and P_{std} are the standard sea-level values of pressure (2116.2 psf) and temperature (288.16 K).

The total pressure and temperature can now be found from equation (18):

$$\left.\begin{aligned} T_{tot} &= T_r * T \\ P_{tot} &= P_r * P \end{aligned}\right\} \tag{20}$$

The compressible and incompressible dynamic pressures are:

$$\left.\begin{aligned} q &= 0.5\ \rho V_a^2 \\ q_c &= P_{tot} - P \end{aligned}\right\} \tag{21}$$

Finally, the equivalent and calibrated airspeeds:

$$\left.\begin{aligned} V_{eq} &= \rho/\rho_{std} * V_a \\ V_{cal} &= V_{sound}\ \sqrt{5\{[1 + (q_c/P_{std})]^{0.2857} - 1\}} \end{aligned}\right\} \tag{22}$$

Wind Model

The wind model includes steady winds and turbulence conforming to the Dryden spectral model. The wind is assumed to be a frozen field of turbulence drifting at a mean wind speed relative to the earth. The turbulence is defined by a characteristic high-frequency cutoff wavelength and a standard deviation which is a function of altitude and intensity category, i.e., light, moderate. The cutoff wavelength is determined by the rotor diameter, as the rotor is assumed to be completely engulfed by each change in the wind from time step to time step. With this assumption the turbulence is generated by simply adding a random component to the velocity vector in body axes, rather than an elaborate integration across the rotor disc.

The changes in the velocity vector enter the force- and moment-generation subroutines and affect the accelerations of the helicopter model. Angular accelerations are simulated by simply adding random increments (conforming to the Dryden model) to the angular velocity components.

All random turbulence effects are removed during trim; however, the mean wind is included. The random velocity changes as a result of turbulence would make it impossible to trim.

The wind model used in the SH-3G simulation is identical to that of SMART (see ref. 6). A background description can also be found in reference 7.

Fuselage Aerodynamics

The fuselage aerodynamic forces and moments are presented as functions of the angle of attack, sideslip angle, and dynamic pressure. The forces and moments are first presented in coefficient form as functions of the two aerodynamic angles. The coefficients are then multiplied by the dynamic pressure and transformed to body axes.

Data for the fuselage aerodynamics model are taken from two sources: a trainer math model of the SH-3H (ref. 8) and a Sikorsky Engineering Report (ref. 9), both prepared under Navy contract. Reference 8 contains equations for the various forces and moments and reference 9 contains actual wind-tunnel test data.

The fuselage aerodynamics submodel has been greatly simplified from the CH-53 subroutine on which it is based. The philosophy has been to use linear or trigonometric functions to approximate the wind-tunnel data when simple equations are not already available. Model accuracy is maintained for small values of the angle of attack and sideslip angle, but no attempt is made to fit the data exactly for large angles. The large angles are, generally, only possible at low airspeeds which means small fuselage forces and moments compared to the rotor aerodynamics. Further sophistication of the model for large aerodynamic angles is therefore not justified.

Fuselage damping moments have also been neglected. This does not substantially harm the fidelity of the simulation because the simulation will almost always be used with the automatic control system on to compensate for the lack of natural damping.

The first parameter to calculate is the effective angle of attack of the fuselage accounting for the main rotor downwash. This local angle of attack is only used in finding the fuselage aerodynamics. The rotor downwash factor (from the CH-53 model) is:

$$e_m = C_{T_m} / 2\sqrt{\lambda_m^2 + \mu_m^2} \tag{23}$$

where C_{T_m} is the main-rotor thrust coefficient, λ_m is the main rotor inflow ratio, and μ_m is the main rotor tip-speed ratio.

The fuselage local angle of attack is:

$$\alpha_\ell = \alpha - e_m e_{kf} \tag{24}$$

where e_{kf} is taken as 0.5 from reference 9.

The following force and moment coefficients, in fuselage wind axes, have the dimensions of square feet. The aerodynamic angles are in degrees.

The side-force coefficient is an approximation to wind-tunnel test data from reference 9:

$$\left.\begin{aligned} C_{F_y} &= -7\beta && |\beta| \le 50 \\ &= -350\ \text{sign}(\beta) && |\beta| > 50 \end{aligned}\right\} \tag{25}$$

The lift-force coefficient is a strong function of both the angle of attack and the sideslip angle. The angle of attack component is taken from the Navy trainer model (ref. 8):

$$C_{F_{L_1}} = 10 + 410\ S(\alpha_\ell) \tag{26}$$

The lift-force coefficient, as a result of sideslip, is a linear approximation of wind-tunnel data from reference 9:

$$\left.\begin{aligned} C_{F_{L_2}} &= -4\ |\beta| && |\beta| < 10 \\ &= -40 && 10 \le |\beta| < 40 \\ &= -7.6 \times |\beta| + 344 && 40 \le |\beta| < 65 \\ &= -150 && |\beta| \ge 65 \end{aligned}\right\} \tag{27}$$

The drag-force coefficient is also a strong function of both angle of attack and sideslip angle. The angle-of-attack component is again taken from the Navy trainer model (ref. 8):

$$C_{F_{D_1}} = C_{F_{D_0}} + 324\ S^2(\alpha_\ell + 2) \tag{28}$$

The flat plate area, $C_{F_{D_0}}$, was determined ad hoc by matching the torque at 90 knots. The value finally used was 44 square feet.

The drag force coefficient because of sideslip is a sinusoidal approximation to Sikorsky wind-tunnel data from reference 9:

$$C_{F_{D_2}} = 500\ S^2(\beta) \tag{29}$$

The following moment coefficients are with respect to body axes and have dimensions of cubic feet. They are all approximations to Sikorsky wind-tunnel test data from reference 9, except for the pitching moment due to angle of attack which is from the Navy trainer model.

The rolling moment due to sideslip is given by:

$$\left.\begin{aligned} C_{M_\beta} &= -4.5\ \beta && |\beta| < 20 \\ &= -90\ \text{sign}(\beta) && |\beta| \ge 20 \end{aligned}\right\} \tag{30}$$

The pitching-moment coefficient has two components: one from angle of attack and another from sideslip. The component due to angle of attack is given by:

$$C_{M_{m1}} = 170 - 1950\ S(\alpha_\ell) \tag{31}$$

The component due to sideslip is

$$C_{M_{m2}} = -175\ S(4 \times |\beta|) \tag{32}$$

The yawing moment due to sideslip is given by

$$\left.\begin{aligned} C_{M_n} &= -400\ S(4.5\ \beta) && |\beta| < 40 \\ &= 80[\beta - 40\ \text{sign}(\beta)] && 40 \le |\beta| < 90 \\ &= 4000 * \text{sign}(\beta) && |\beta| \ge 90 \end{aligned}\right\} \tag{33}$$

The fuselage forces are found by multiplying the force coefficients by the dynamic pressure which is given by

$$q = 0.5\ \rho V_a^2 \tag{34}$$

The forces are then given by:

$$\left.\begin{aligned} Y &= C_{F_Y} q \\ L_F &= \left(C_{F_{L1}} + C_{F_{L2}}\right) q \\ D &= \left(C_{F_{D1}} + C_{F_{D2}}\right) q \end{aligned}\right\} \tag{35}$$

In wind axes:

$$\begin{pmatrix} F_{a_x} \\ F_{a_y} \\ F_{a_z} \end{pmatrix}_w = \begin{pmatrix} -D \\ Y \\ -L_f \end{pmatrix} \tag{36}$$

The wind-axis forces are transformed to body axes as follows:

$$\begin{pmatrix} F_{a_x} \\ F_{a_y} \\ F_{a_z} \end{pmatrix}_b = \begin{vmatrix} C\alpha C\beta & -C\alpha S\beta & -S\alpha \\ S\beta & C\beta & 0 \\ S\alpha C\beta & -S\alpha S\beta & C\alpha \end{vmatrix} \begin{pmatrix} F_{a_x} \\ F_{a_y} \\ F_{a_z} \end{pmatrix}_w \tag{37}$$

The fuselage moments, in body axes, are found by multiplying the dynamic pressure times the moment coefficients.

$$\left.\begin{aligned} T_{a_\ell} &= C_{M_\ell} q \\ T_{a_m} &= \left(C_{M_{m1}} + C_{M_{m2}}\right) q \\ T_{a_n} &= C_{m_n} q \end{aligned}\right\} \tag{38}$$

Main-Rotor Model

The main-rotor model is adapted from the CH-53 version (see ref. 4), which is a classical nonlinear Bailey model assuming uniform inflow. An empirical method to account for nonuniform inflow using flight-test data has been included in the SH-3G rotor models.

The main-rotor and tail-rotor models are based on the following assumptions:

1. Compressibility and stall effects can be neglected.
2. Lag effects can be neglected.
3. Only the first harmonic motion of the rotor blades is important.
4. Blade coning and flapping angles are quasi-static.
5. Any wind or turbulence emerses the entire rotor disk at once.

The following discussion is paraphrased from reference 4 (for completeness) with the exception of the torque equation.

The airspeed of the entire rotor disc is assumed to be that of the rotor hub. The airspeed at the rotor hub is calculated in shaft axes using the helicopter airspeed and angular velocity.

$$\begin{pmatrix} U_s \\ V_s \\ W_s \end{pmatrix} = \begin{vmatrix} C\theta_s & 0 & -S\theta_s \\ S\theta_s S\phi_s & C\phi_s & C\theta_s S\phi_s \\ S\theta_s C\phi_s & -S\phi_s & C\theta_s C\phi_s \end{vmatrix} \begin{pmatrix} U_b \\ V_b \\ W_b \end{pmatrix} + \begin{vmatrix} 0 & z_h & -y_h \\ -z_h & 0 & x_h \\ y_h & -x_h & 0 \end{vmatrix} \begin{pmatrix} P \\ Q \\ R \end{pmatrix} \tag{39}$$

where θ_s is the shaft pitch angle; ϕ_s is the shaft roll angle; x_h, y_h, z_h are the hub coordinates in body axes; and U_b, V_b, and W_b are the body-axis velocities.

The airspeed at the hub is transferred into control axes using the rotor orientation angle:

$$\beta_r = \arctan\left(\frac{V_s + A_{1_s} W_s}{U_s + B_{1_s} W_s}\right) \tag{40}$$

which is obtained using the definition of control axes: $V_c = 0$.

Using small angle approximations for the main rotor cyclic control inputs (swashplate angles), A_{1_s} and B_{1_s}:

$$\begin{pmatrix} U_c \\ V_c \\ W_c \end{pmatrix} = \begin{vmatrix} C\beta_r & S\beta_r & B_{1_S}C\beta_r + A_{1_S}S\beta_r \\ -S\beta_r & C\beta_r & A_{1_S}C\beta_r - B_{1_S}S\beta_r \\ -B_{1_S} & -A_{1_S} & 1 \end{vmatrix} \begin{pmatrix} U_s \\ V_s \\ W_s \end{pmatrix} \tag{41}$$

The Bailey method requires three parameters on each iteration: tip-speed ratio, inflow ratio, and the rotor pitch. The tip-speed and inflow ratios are defined as:

$$\left.\begin{aligned} \mu &= U_c/\Omega R \\ \lambda &= W_c/\Omega R - \nu \end{aligned}\right\} \tag{42}$$

where Ω is the angular velocity of the rotor, R is the blade radius, and ν is the induced inflow ratio.

The induced inflow ratio, ν, is found by filtering the steady-state value, an idea first used by Schaughnessy (ref. 1). The resulting first-order, nonlinear differential equation is more stable numerically than algebraic calculations.

$$\dot{\nu} = \frac{1}{\tau_\nu}\left(\frac{C_T}{\sqrt{\mu^2 + \lambda^2}} - \nu\right) \tag{43}$$

The thrust coefficient is C_T and τ_ν is an empirical time constant to simulate the lag associated with inflow changes.

The rotor thrust coefficient, C_T, and the coning angle a_0 (see fig. 8) are calculated by equations from ref. 4. These equations are simplified versions of those found in Bailey's NACA report (ref. 2).

$$\left.\begin{aligned} C_T &= \frac{\sigma a}{2}\left[\left(\frac{1}{2}B^2 + \frac{1}{4}\mu^2\right)\lambda + \left(\frac{1}{3}B^3 + \frac{1}{2}B\mu^2 - \frac{4}{9\pi}\mu^3\right)\theta_0 + \left(\frac{1}{4}B^4 + \frac{1}{4}B^2\mu^2\right)\theta_1\right] \\ a_0 &= \gamma\left[\left(\frac{1}{6}B^3 + 0.04\mu^3\right)\lambda + \left(\frac{1}{8}B^4 + \frac{1}{8}B^2\mu^2\right)\theta_0 + \left(\frac{1}{10}B^5 + \frac{1}{12}B^3\mu^2\right)\theta_1\right] \end{aligned}\right\} \tag{44}$$

where σ is the solidity ratio, γ is a blade mass constant, B is the tip loss factor, θ_0 is the rotor pitch, θ_1 is the rotor twist, and a is the blade-lift curve slope. The blade-lift curve slope is usually taken as 5.73/rad based on two-dimensional, wind-tunnel data and the resulting thrust coefficient is usually optimistic. For the present simulation, the blade-lift curve slope was determined empirically by decreasing its value until the simulation collective stick position in hover, matched flight-test data from reference 5. The final value was 5.2/rad.

The calculation of the rotor flapping angles (see fig. 9) requires the fuselage angular velocity in control axes. This requires the following two transformations: from body to shaft axes and from shaft to control axes.

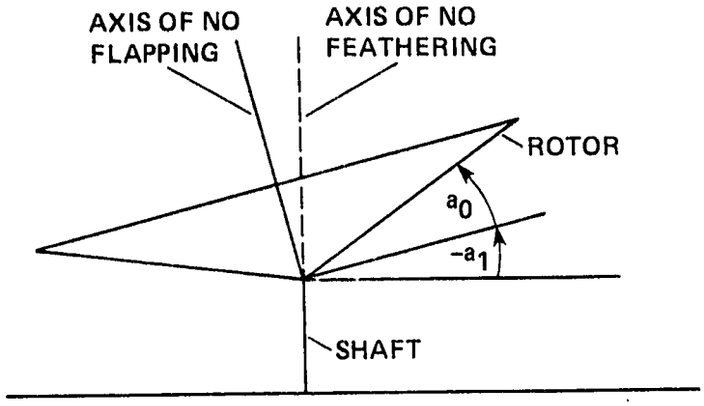

Figure 8.- Coning angle.

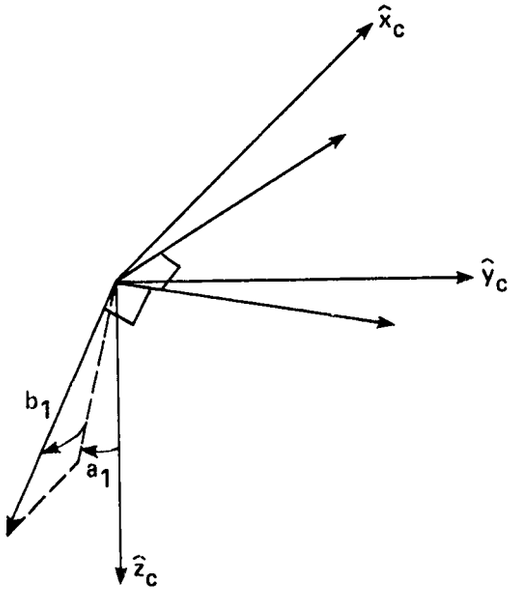

Figure 9.- Flapping angles.

$$\left.\begin{aligned}
\begin{pmatrix} P_s \\ Q_s \\ R_s \end{pmatrix} &= \begin{vmatrix} C\theta_s & 0 & -S\theta_s \\ S\theta_s S\phi_s & C\phi_s & C\theta_s S\phi_s \\ S\theta_s C\phi_s & -S\phi_s & C\theta_s C\phi_s \end{vmatrix} \begin{pmatrix} P \\ Q \\ R \end{pmatrix} \\
\begin{pmatrix} P_c \\ Q_c \\ R_c \end{pmatrix} &= \begin{vmatrix} C\beta_r & S\beta_r & B_{1_s} C\beta_r + A_{1_s} S\beta_r \\ -S\beta_r & C\beta_r & A_{1_s} C\beta_r - B_{1_s} S\beta_r \\ -B_{1_s} & -A_{1_s} & 1 \end{vmatrix} \begin{pmatrix} P_s \\ Q_s \\ R_s \end{pmatrix}
\end{aligned}\right\} \quad (45)$$

The flapping angles a_1 and b_1 are calculated in control axes by formulas from reference 1:

$$\left.\begin{aligned}
a_1 &= \frac{1}{1 - \frac{\mu^2}{2B^2}} \left[\left(2\lambda + \frac{8}{3}\theta_{0.75} \right)\mu + \frac{P_c}{\Omega} - \frac{16 Q_c}{B^4 \gamma \Omega} \right] \\
b_1 &= \frac{1}{1 - \frac{\mu^2}{2B^2}} \left(\frac{4}{3}\mu a_0 - \frac{Q_c}{\Omega} - \frac{16 P_c}{B^4 \gamma \Omega} \right)
\end{aligned}\right\} \quad (46)$$

where $\theta_{0.75}$ is the blade pitch at 75% of the rotor radius, i.e.,

$$\theta_{0.75} = \theta_0 + 0.75\ \theta_1$$

The rotor drag force in wind axes is given by:

$$H = T*a'$$

where a' represents a lift-induced, tilt back angle of the rotor thrust vector and is given by (ref. 1):

$$a' = \frac{1}{1 - \frac{\mu^2}{2B^2}} \left[\left(2\lambda + \frac{8}{3} \theta_{0.75} \right) \mu - \frac{24 Q_c}{B^4 \gamma \Omega} \left(1 - \frac{0.29\ \theta_{0.75}}{\frac{C_T}{\sigma}} \right) \right] \tag{47}$$

The Q_c term accounts for fuselage pitch rate.

The torque equation is taken from page 151, equation (5.27a) in reference 3:

$$C_q = \frac{\delta \sigma}{8} (1 + K_{sw} \times 3\mu^2) + C_T (K_{nu} \nu - \lambda - \mu a') \tag{48}$$

where K_{sw} is a constant to approximately account for spanwise flow in forward flight, K_{nu} similarly accounts for nonuniform inflow, and δ is the blade profile drag coefficient K_{sw} and K_{nu} were determined as follows:

K_{sw} = 1.57 (attributed to Stepniewsky in ref. 3, p. 151)

K_{nu} = 0.15 (empirically determined by matching the simulation torque in hover to flight-test data from ref. 5)

The Bailey report (ref. 2) gives δ as:

$$\delta = \delta_0 + \delta_1 \alpha_r + \delta_2 \alpha_r^2 \tag{49}$$

where $\alpha_r = 6C_T/(\sigma a)$ which is the average blade angle of attack in hover. For the NACA 0012 airfoil and calculated from reference 10 $\delta_0 = 0.0078$, $\delta_1 = -0.0090$, and $\delta_2 = 0.2987$.

The torque is calculated from the definition of torque coefficient as:

$$Q_a = bcR^2 \rho (R\Omega)^2 \frac{C_q}{\sigma} \tag{50}$$

where b is the number of blades and c is the blade chord.

The rotor side force is defined in terms of the rotor-side-force coefficient:

$$J = bcR\rho (R\Omega)^2 \frac{C_y}{\sigma} \tag{51}$$

where

$$C_y = \frac{\sigma a}{2} \left[\frac{3}{4} b_1 \lambda - \frac{3}{2} a_0 \mu \lambda + \frac{1}{4} a_1 b_1 \mu - a_0 a_1 \mu^2 + \frac{1}{6} a_0 a_1 - \left(\frac{3}{4} \mu a_0 - \frac{1}{3} b_1 - \frac{1}{2} \mu^2 b_1 \right) \theta_{0.75} \right] \tag{52}$$

This last equation is from reference 4 and was used on the CH-53.

The rotor forces are transformed from control axes to body axes by using the transposes of the matrices in equations (45). First transform control to shaft axes:

$$\begin{pmatrix} F_{x_s} \\ F_{y_s} \\ F_{z_s} \end{pmatrix}_m = \begin{vmatrix} C\beta_r & -S\beta_r & -B_{1_s} \\ S\beta_r & C\beta_r & -A_{1_s} \\ B_{1_s}C\beta_r + A_{1_s}S\beta_r & A_{1_s}C\beta_r - B_{1_s}S\beta_r & 1 \end{vmatrix} \begin{pmatrix} -H \\ J \\ -T \end{pmatrix}_m \tag{53}$$

Then transform from shaft axes to body axes:

$$\begin{pmatrix} F_x \\ F_y \\ F_z \end{pmatrix}_m = \begin{vmatrix} C\theta_s & S\theta_s S\phi_s & S\theta_s C\phi_s \\ 0 & C\phi_s & -S\phi_s \\ -S\theta_s & C\theta_s S\phi_s & C\theta_s C\phi_s \end{vmatrix} \begin{pmatrix} F_{x_s} \\ F_{y_s} \\ F_{z_s} \end{pmatrix}_m \tag{54}$$

The rotor cyclic controls enter the main rotor model through the cyclic flapping angles. From reference 4, these angles in shaft axes are given by:

$$\begin{pmatrix} a_{1_s} \\ b_{1_s} \end{pmatrix} = \begin{vmatrix} C\beta_r & S\beta_r \\ -S\beta_r & C\beta_r \end{vmatrix} \begin{pmatrix} a_1 \\ b_1 \end{pmatrix} + \begin{pmatrix} -B_{1_s} \\ A_{1_s} \end{pmatrix} \tag{55}$$

Pure pitching and rolling moments about the hub are generated by the flapping hinge offsets. A pure yawing moment is generated by the engine torque. In shaft axes these pure moments are given by (ref. 4):

$$\begin{pmatrix} L_s \\ M_s \\ N_s \end{pmatrix} = 0.5\ e\Omega^2 m_w \begin{pmatrix} b_{1_s} \\ a_{1_s} \\ 0 \end{pmatrix} + \begin{pmatrix} 0 \\ 0 \\ Q_e \end{pmatrix} \tag{56}$$

where e is the flapping hinge offset, m_w is the blade mass moment, and Q_e is the engine torque.

The total moments of the main rotor in body axes result from the pure moments (converted to body axes) plus the rotor forces acting through the coordinates of the rotor hub relative to the center of gravity:

$$\begin{pmatrix} L \\ M \\ N \end{pmatrix} = \begin{vmatrix} C\theta_s & S\theta_s S\phi_s & S\theta_s C\phi_s \\ 0 & C\phi_s & -S\phi_s \\ -S\theta_s & C\theta_s S\phi_s & C\theta_s C\phi_s \end{vmatrix} \begin{pmatrix} L_s \\ M_s \\ N_s \end{pmatrix} + \begin{vmatrix} 0 & -z_h & y_h \\ z_h & 0 & -x_h \\ -y_h & x_h & 0 \end{vmatrix} \begin{pmatrix} F_x \\ F_y \\ F_z \end{pmatrix}_m \tag{57}$$

where x_h, y_h, and z_h are the coordinates of the rotor hub relative to the center of gravity.

The main-rotor angular acceleration is found by summing the torques at the hub:

$$\dot{} = (Q_e - Q_a - Q_t \cdot G_r)/I_m \tag{58}$$

where Q_t is the tail-rotor torque, G_r is the gear ratio between the main rotor and tail rotor ($G_r > 1$), and I_m is the moment of inertia of the rotor blades and hub.

Tail Rotor Model

For the most part, the tail-rotor model calculates forces and moments in the same manner as the main-rotor model. The tail rotor does not have cyclic-control angle commands. The tail rotor does, however, have a δ_3 hinge, which has the effect of increasing the stiffness and natural frequency of tail-rotor flapping.

The equation for tail-rotor pitch from reference 4 is given by:

$$\theta_{0t} = \theta_{ct} - a_{0t} \tan(\delta_3) \tag{59}$$

where θ_{ct} is the commanded tail-rotor collective and δ_3 is the lag offset angle. Notice that the tail-rotor pitch is coupled to the coning angle, a_{0t}. Since equations (44) and (59) are now coupled, they should be solved simultaneously. Eliminating a_{0t} between these two equations yields:

$$\theta_{0t} = \frac{\theta_{ct} - (Z_1 \lambda_t + Z_3 \theta_{1t}) \tan \delta_3}{1 + Z_2 \tan \delta_3} \tag{60}$$

where Z_1, Z_2, and Z_3 are defined from equations (44) by:

$$a_{0t} = Z_1 \lambda_t + Z_2 \theta_{0t} + Z_3 \theta_{1t} \tag{61}$$

Engine Model

The SH-3G uses two T38-GE-8F gas turbine engines operating together except, of course, in the event of engine failure. Each engine has a gas-generator section providing compressed air for a free or power-turbine section. An engine governor controls fuel flow to maintain constant power-turbine speed under changing loads. Fuel flow primarily affects the gas-generator speed which controls the torque applied to the power turbine.

The governor is limited in a complex way during engine acceleration or deceleration to avoid the following undesirable conditions: (1) turbine overtemperature, (2) compressor stall, (3) overrich flameout, or (4) overlean flameout. These limits are in direct opposition to obtaining maximum power and immediate response. The net result to the pilot is: ". . . engine response to new power or speed settings is not instantaneous: a few seconds must be allowed for the engine to stabilize at the new condition" (ref. 11, p. 1-10).

A very important engine characteristic to simulate is this delay to sudden changes in the power required. A simple and effective way to model the engine is as a torque device regulating main rotor rpm. The main rotor is then modeled approximately as a pure inertia and the controller is an application of pseudo-derivative feedback in a simple form (ref. 12).

Figure 10 shows a block diagram of the engine/governor model. As developed in reference 12, the characteristic equation is:

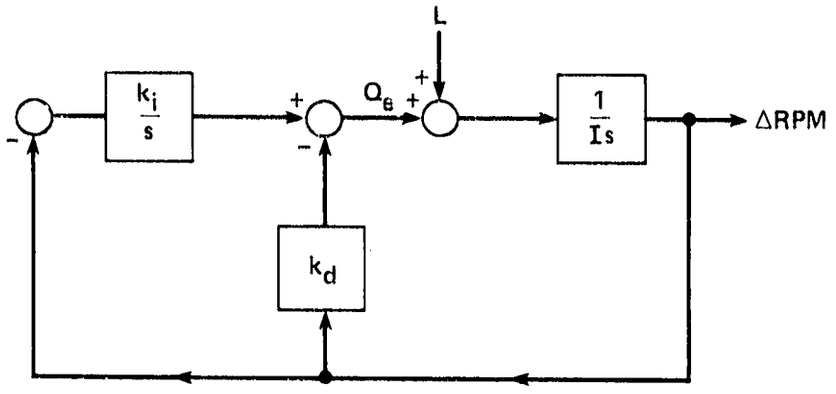

Figure 10.- Engine and governor model.

$$Is^2 + K_d s + K_i = 0 \tag{62}$$

where d stands for derivative and i for integral.

If equation (62) is critically damped, then the response to a step load, L_0, is:

$$X = \frac{L_0}{K_i}\left[1 - \left(1 + \frac{K_d}{2I}\,t\right)e^{-(K_d/2I)t}\right] \tag{63}$$

This implies a characteristic time:

$$\tau = \frac{2I}{K_d} \tag{64}$$

Now from reference 8, the inertia of the main rotor and hub is 10,190 slug-ft^2 or $I = 1067$ ft-lb-sec/rpm. If τ is chosen as 1.5 sec to simulate the engine delay, then $K_d = 1423$ ft-lb/rpm. Critical damping determines K_i as 474 ft-lb/rpm-sec.

The engine model is summarized by:

$$\left.\begin{aligned} \Delta RPM &= RPM - 203.3 \\ \textstyle\int RPM &= \textstyle\int RPM + \Delta RPM \times DT \\ Q_e &= K_i \textstyle\int RPM + K_d(\Delta RPM) \end{aligned}\right\} \tag{65}$$

where

ΔRPM deviation of main-rotor rpm from the nominal of 203.3

$\int RPM$ integral of rpm error

DT cycletime

Q_e engine torque

Control System and Rigging

The SH-3G flight-control-system model consists of rigging information, the automatic stabilization equipment (ASE) model, and the barometric altitude hold mode. Rigging is the mechanical gain, including coupling, between the pilot's controls and the motion of the swashplate, i.e., collective stick (in.) to collective pitch (deg). The automatic control system has four channels of stabilization: the collective, the pitch, the roll and the yaw channels. The SH-3G is attitude-stabilized in pitch and roll. The yaw channel is a heavy yaw damper plus heading hold control by microswitches on the rudder pedals. The barometric altitude hold mode is controlled by a separate switch from the ASE and drives the collective channel.

The rigging constants are taken for the most part from reference 13, the SH-3G maintenance manual. The ASE is taken chiefly from reference 8, the Navy trainer math model with some clarification from reference 11, the Navy flight manual.

The SH-3G has four pilot controls: collective stick, lateral stick, longitudinal stick, and rudder pedals which control the main rotor collective pitch, the lateral flapping angle, the longitudinal flapping angle, and the tail rotor collective, respectively.

Each pilot control has physical travel limits as detailed in table 1. Each controlled parameter, i.e., tail-rotor collective, also has physical limits as shown in table 2.

TABLE 1.- PHYSICAL LIMITS OF THE PILOT's CONTROLS (in.)

Control	Lower limit	Upper limit	Sign convention
Collective stick	0.00	7.46	+ UP
Lateral cyclic stick	-7.00	7.00	+ RIGHT
Longitudinal cyclic stick	-7.54	6.46	+ AFT
Rotary rudder pedals	-3.25	3.25	+ NOSE RIGHT

TABLE 2.- PHYSICAL LIMITS OF THE MAIN ROTOR AND TAIL ROTOR (deg)

Rotor parameter	Lower limit	Upper limit	Sign convention
Main rotor collective pitch	8.10	19.50	+ UP
Lateral flapping angle	-9.10	6.90	+ RIGHT
Longitudinal flapping angle	-15.35	10.15	+ FWD
Tail rotor collective pitch	-6.50	25.00	+ NOSE LEFT

The form of the rigging equations are shown below:

$$\left.\begin{aligned} \theta_0 &= \theta_{0,0} + K_c X_c + ASE_c \\ A_{1_s} &= K_{1a} X_{1a}\, C\psi_0 - K_{1o} X_{1o}\, S\psi_0 + K_{1a\text{-}c} X_c + ASE_{1a} \\ B_{1_s} &= K_{1a} X_{1a}\, S\psi_0 + K_{1o} X_{1o}\, C\psi_0 + K_{1o\text{-}c} X_c + ASE_{1o} \\ \theta_{0t} &= \theta_{0t,0} + K_t X_t + K_{t\text{-}c} X_c + ASE_t \end{aligned}\right\} \quad (66)$$

where X_c, X_{1a}, X_{1o}, and X_t are the collective stick, the lateral cyclic-stick, the longitudinal cyclic-stick, and the rudder-pedal positions, respectively, in inches. Note the coupling between collective and the other three controls. The cyclic control phase angle ψ_0, resulting from the rotor hinge offset, has been calculated by equations in appendix H of reference 14. The rigging constants are shown in table 3.

Each of the ASE components in equations (66) are limited to 10% control authority as shown in table 4:

TABLE 3.- RIGGING CONSTANTS

Constant	Value	Units
ψ_0	2.72	deg
$\theta_{0,0}$	8.10	deg
$\theta_{0t,0}$	9.25	deg
K_c	1.528	deg/in.
K_{1a}	1.143	deg/in.
K_{1o}	-1.821	deg/in.
K_t	-4.846	deg/in.
$K_{c\text{-}1a}$	-0.1475	deg/in.
$K_{c\text{-}1o}$	-0.3485	deg/in.
$K_{c\text{-}t}$	1.135	deg/in.

TABLE 4.- ASE AUTHORITY

Channel	Limits, deg	Symbol
Collective	±1.14	ASE_c
Lateral	±1.60	ASE_{1a}
Longitudinal	±2.55	ASE_{1o}
Yaw	±3.25	ASE_t

The control system equations are shown below:

$$\left.\begin{aligned} ASE_c &= [G_{bah}(h - h_{ref}) + G_c X_c] S_{bah} S_{ase} \\ ASE_{1a} &= \left(G_p P + G_\phi \phi \frac{G_{1a} X_{1a}}{\tau_{x_{1a}} s + 1}\right) \frac{S_{ase}}{\tau_{1a} s + 1} \\ ASE_{1o} &= (G_\theta \theta + G_Q Q) \frac{S_{ase}}{\tau_{1o} s + 1} \\ ASE_t &= \frac{G_R R + G_\psi (\psi - \psi_{ref})}{\tau_t s + 1} \end{aligned}\right\} \quad (67)$$

OF POOR QUALITY

where

S_{bah} barometric altitude hold switch (1 = on)

S_{ase} automatic stabilization switch (1 = on)

h_{ref} barometric altitude reference: set when the barometric altitude hold switch is on

$\tau_{x_{1a}}, \tau_{1a}, \tau_{1o}, \tau_t$ time constants for first order filters

ψ_{ref} heading reference: set when feet off the rudder pedals

P,R body axis and yaw rates, respectively

s Laplace Transform variable

The control system gains and time constants are shown in table 5:

TABLE 5.- CONTROL SYSTEM GAINS AND TIME CONSTANTS

Constant	Value	Units
$\tau_{x_{1a}}$	0.8	sec
τ_{1a}	.625	sec
τ_{1o}	.625	sec
τ_t	.3125	sec
G_c	.1430	deg/in.
G_{bah}	-.01238	deg/ft
G_ϕ	-.1006	deg/deg
G_p	-.1187	deg/(deg/sec)
$G_{x_{1a}}$	1.515	deg/in.
G_θ	.2401	deg/deg
G_Q	.2593	deg/(deg/sec)
G_{1o}	-.4504	deg/in.
G_R	.2428	deg/(deg/sec)
G_ψ	1.3	deg/deg

The lateral and longitudinal channels are filtered to prevent sharp transients when the ASE is switched on.

The actuator dynamics have been neglected in the control model because of the relatively short time constants involved (<0.2 sec).

TRIM METHOD

The trim algorithm used is adapted from BQUIET, a general trimming subroutine for simulations at NASA Ames and documented in reference 15. BQUIET nulls six states with six or less controls by: (1) finding perturbations in the six states for each

control, (2) extrapolating linearly to find a new control vector which will minimize the state vector in the least-squares sense, and (3) iterating until the states are within some tolerance of zero. Recognizing that the math model to be trimmed may be highly nonlinear, (2) is modified by a "gradient gain" of 0.5, i.e., the extrapolation is only carried out half way. This damps oscillations about the solution and can prevent divergence.

The BQUIET algorithm has been simplified and tailored for the SH-3G simulation. This required initializing the program properly between perturbations, choosing the controls and states, and making certain improvements in the details of the algorithm.

Trim Initialization

The SH-3G trim algorithm requires an estimate of the partial derivative of each state with respect to each control on every iteration. The partials are found by choosing a reference control vector, evaluating the corresponding reference state vector, disturbing each control in turn by a small percentage of its travel, and evaluating the change in the state vector from the reference. The state vector is evaluated by setting initial conditions of the math model (including the controls), allowing the model to "fly" for two shortened cycles, and observing the states. The trim cycle time is chosen very short so that integrals present in the math model will effectively not operate in trim mode, avoiding the need for special loops around each integrator in trim. Filters, however, must be set to their steady-state-gain value while trimming or they will be unaffected by changes in the controls.

Ordinarily, the linear accelerations along the body axes and the angular accelerations about the body axes are chosen as states to be "trimmed." All position, velocity, attitude, and angular velocity variables must therefore be set at the desired trim values before each pass through the math model to determine the accelerations. Since, in this math model, two of the controls are attitude variables, this initialization must be recalculated before every pass.

The initial velocities and attitudes need to be specified in body axes as well as in inertial axes. For the convenience of the researcher, sideslip angle, flight-path angle, the equivalent velocity (knots), and the wind vector should be specifiable. The bank angle and angle of attack are appropriate control variables and are, therefore, also specified. The problem may be stated formally as: given: α, β, γ_v, γ_h, $\bar{W}$, V_a, ϕ, find: $\bar{V}_b$, $\bar{V}$, θ, ψ. See appendix A for the solution.

In addition, the model should be trimmable in hover, rearward flight, vertical climb and descent, and sideward flight. These problems are also addressed in appendix A.

Trim States and Controls

The classical Newton's method of finding the zeroes of a function consists of finding the slope of the function at a trial point, extrapolating linearly to zero, evaluating the function at the new trial point, and repeating. For this application, this method is extended to many dimensions and the extent of extrapolation is controlled by a "gradient" gain.

The original algorithm from BQUIET assumes an overdetermined set of linear equations, i.e., fewer controls than states. To avoid the possibility of uncontrollable

states and to simplify the computation, the present trim method insists on as many controls as states. This results in a square matrix of partial derivatives of the states with respect to the controls. Mathematically:

$$X = Ju \quad \text{where} \quad J_{ij} = \frac{\partial X_i}{\partial u_j}$$

The SH-3G math model originally trimmed six states consisting of the linear accelerations along the body axes and the angular accelerations about the body axes. The six controls were: the initial angle of attack, the initial bank angle, longitudinal cyclic stick, lateral cyclic stick, rotary rudder-pedal position, and collective stick. Trimming improved dramatically with the addition of the main-rotor angular acceleration as a seventh state and the initial value of the engine model filter as a seventh control.

A trim iteration, then, contains eight passes through the math model. Each of the first seven passes fills one column of the square seven by seven matrix of partial derivatives, the Jacobian. Each column of the Jacobian corresponds to perturbations in the states due to a 0.01% of travel change in one control. After the seventh pass, the Jacobian is inverted and multiplied by the current reference state times the gradient gain to produce a new reference control vector. The eighth pass through the math model determines the new reference state vector which should be closer to trim. If the states are less than some trim criteria, the process is stopped. Mathematically:

$$\delta u = -GJ^{-1}X \; ; \quad \text{until} \quad |X_i| < \varepsilon_i \; ; \quad 0 < G < 1$$

Trim Algorithm Improvements

Three minor improvements have been made in the BQUIET algorithm. The improvements involve the limits on control changes, control restrictions when near the boundaries of their travel, and variations in the gradient gain. With these improvements the final math model trims at any airspeed from -30 knots to 135 knots and is fairly insensitive to the initial control guess.

Some limit must be placed on the allowable change in each control, otherwise the trim process may converge very slowly or not at all. The SH-3G trim evaluates the new proposed change in the control vector, finds the control with the largest change as a percentage of its travel, limits this control to 10%, and re-scales the other controls to preserve the direction of the new control vector.

If a control is allowed to exceed its travel, highly nonlinear response to perturbations is likely because of physical limits and mechanical stops modeled. The SH-3G trim, after limiting the change in the control vector as above, makes a further check to see if any control would exceed its travel. If so, that control is limited to half the remaining travel and the control change vector is re-scaled. This is similar to what happens in American football when a 15 yard penalty is called against the offense and less than that remains to the goal line. This allows trimming arbitrarily close to the control limits.

The gradient gain, mentioned earlier, is a measure of the extent of extrapolation of the Jacobian matrix calculated on each iteration in trim. The ad hoc value for the gradient gain used in BQUIET is 0.5. Occasionally, this value is too large,

causing oscillations and even divergence. The oscillations are evident by sign changes in the states after an iteration, so an algorithm using this fact has been devised. Basically, if there are any sign changes after an iteration, the gradient gain is reduced; if there are no sign changes the gradient gain is increased. This reduces oscillations at the beginning of trim and speeds up the convergence at the end near the solution.

MODEL VALIDATION

The SH-3G math model validation is a comparison to Navy flight-test data collected to validate their own trainer simulation of the SH-3H (ref. 5). Various trimmed control positions and time histories were selected to check the SH-3G math model fidelity both statically and dynamically.

Static Checks

Engine torques and trimmed control positions are validated for airspeeds varying from -30 knots to +135 knots. Trimmed control positions are also checked for sideslip angles varying from -25° to +25° at 70 knots nominal airspeed. General flight conditions validated were from 16,000- to 20,000-lb gross weight and sea level to 2,000 ft altitude. The results are presented in figures 11 to 15.

Figure 11 shows engine torque versus airspeed for level forward flight from 40 knots to 135 knots. A comparison between the math model and the flight data is shown for the medium gross weight of 17,764 lb. For airspeeds between 70 and

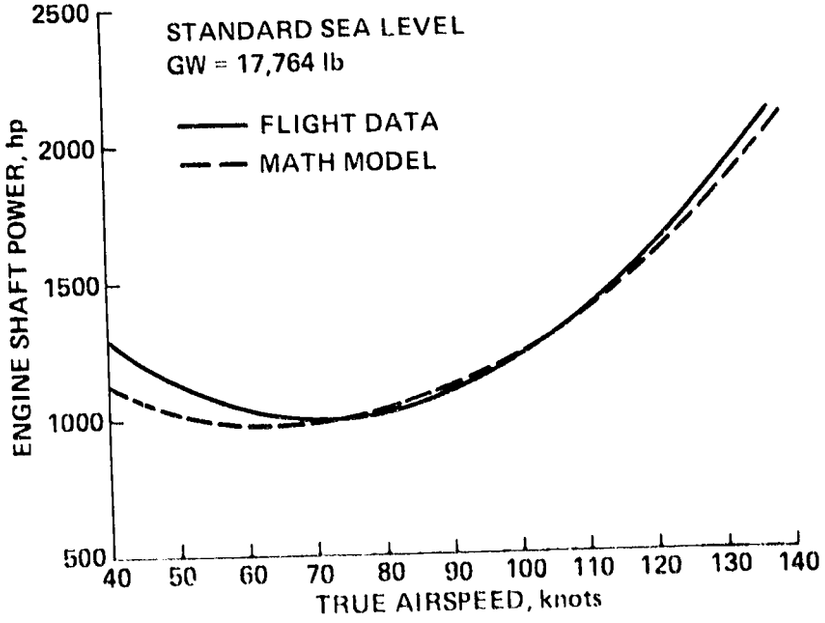

Figure 11.- Level flight performance.

120 knots the torques are almost identical, but the math model is optimistically low below 70 knots and above 120 knots. At 40 knots the discrepancy is largest, probably because of a mismatch in blade profile drag.

Low speed and hover performance is shown in figure 12. Indicated torque for airspeeds from 30 knots aft or rearward to 40 knots forward is plotted for both the math model and the flight test. As can be seen, the flight data are somewhat scattered. It does appear, however, that the math model is a few percent low especially in hover and rearward flight.

Figures 13(a) and 13(b) compare the trimmed control positions for airspeeds from 30 knots to 130 knots in forward flight. The sideslip angle has been matched to the flight-test data for each airspeed.

The collective position shows good agreement between flight test and math model. The minimum collective position falls at 60 knots for the math model, which may be low depending on how the scatter in the flight data is read. This would explain, however, why the math model collective positions are high above 60 knots and low below 60 knots, i.e., a better match might be obtained by shifting the math model curve to the right, corresponding to an increase in induced power and a decrease in flat-plate drag power.

The lateral and longitudinal cyclic positions of the math model agree fairly well with the flight-test data, not varying more than about 7%. The longitudinal sensitivity of the math model is slightly higher than the flight data. The math model lateral cyclic shows a decreasing trend while the flight data increase, although the downward curvature of the two curves is similar.

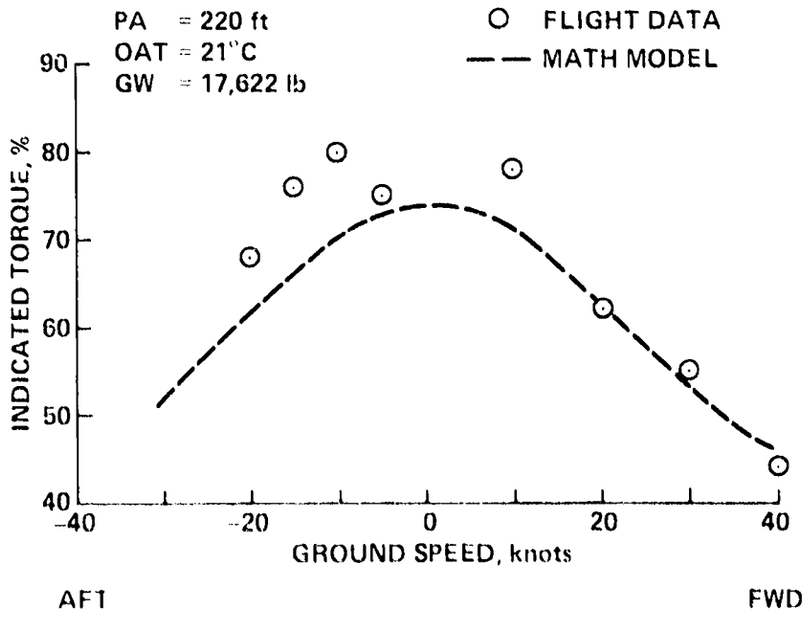

Figure 12.- Low speed performance.

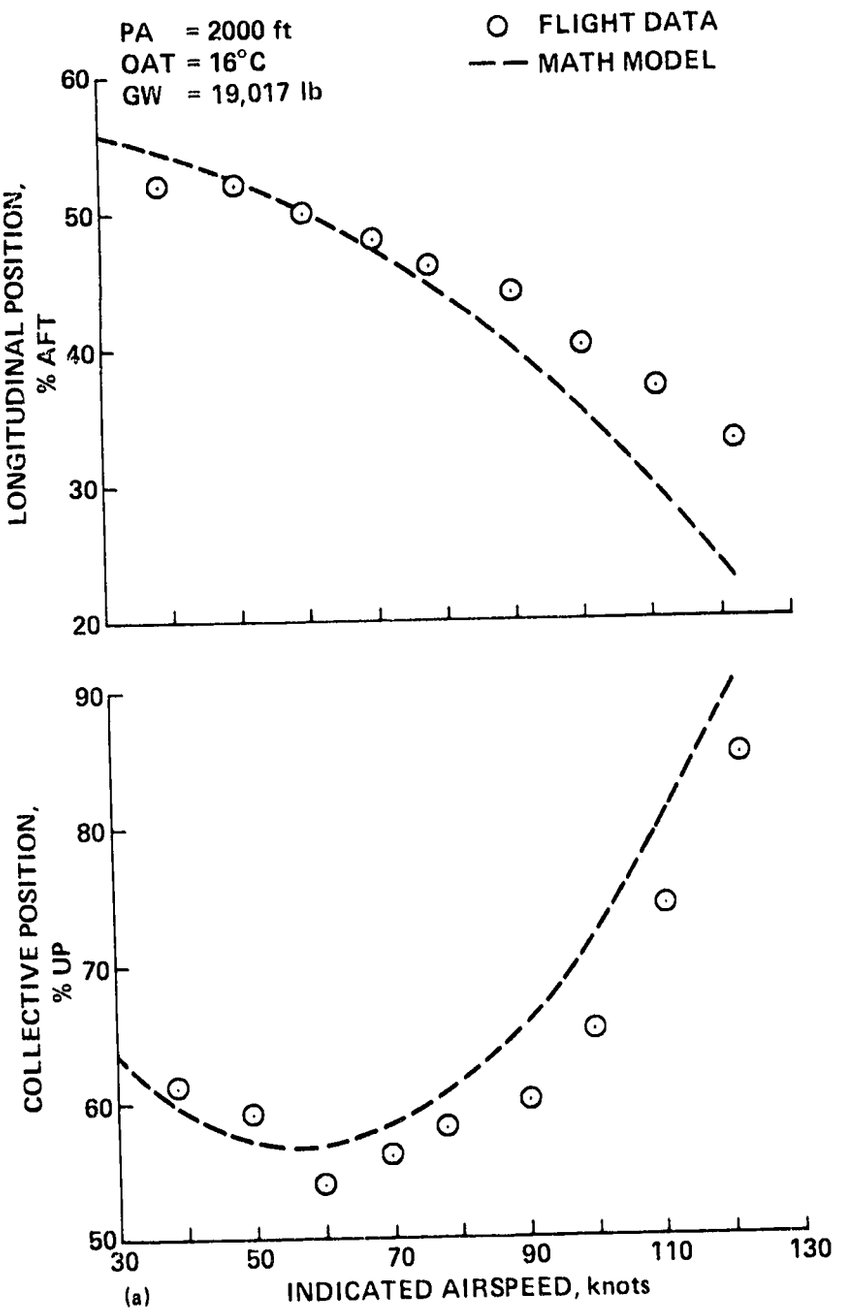

Figure 13.- Forward flight trimmed control positions.

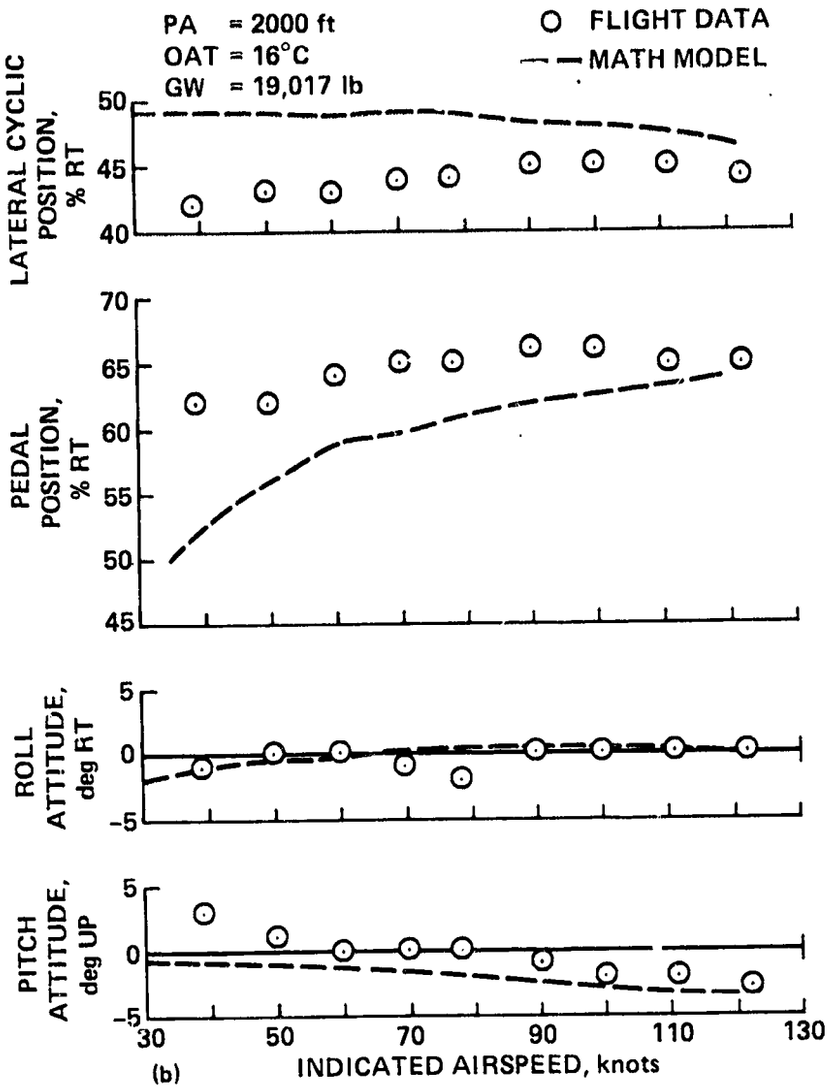

Figure 13.- Concluded.

The math model trimmed pedal position shows the correct trend but the wrong magnitude; being low by as much as 10%. This corresponds to a pedal displacement of 5/8 of an inch, so it is questionable whether a pilot would notice the discrepancy.

The pitch and roll attitudes show the correct trend. The trimmed roll attitudes are virtually indistinguishable between the math model and flight data; the pitch attitudes are a few degrees low.

Figures 14(a) and (b) show the low speed and hover trimmed-control positions. Note that figures 13 and 14 are not comparable because of the large variation in gross weight. The effect of this can be seen in the collective position at 40 knots. In figures 13 the collective position is about 60% corresponding to the gross weight of 19,017 lb as opposed to about 50% and 17,622 lb in figures 14.

Again there is good agreement between the math model and flight data for the collective position and the roll and pitch attitudes. The lateral and longitudinal

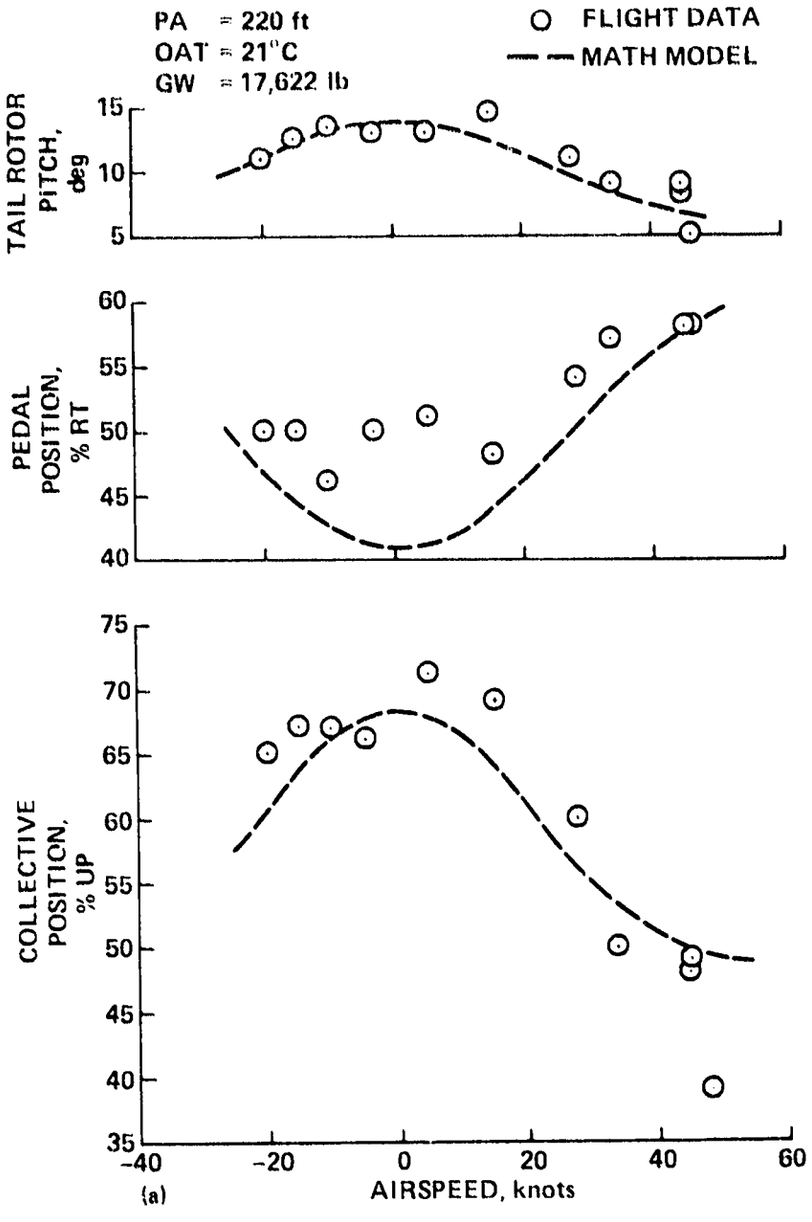

Figure 14.- Low speed trimmed control positions.

cyclic positions also show the correct trends and do not differ from the flight data by more than about 7%. The longitudinal sensitivity of the math model is now less than the flight data in contrast to figures 13. This is probably due to slight differences in center of gravity position which is fixed in the math model.

The math model trimmed pedal position is again low compared to the flight data although the trend appears correct. The pedal position is probably about 5% low on average as it was in figures 13. This error is within reason, as the SH-3G can be adjusted mechanically by as much as 10%.

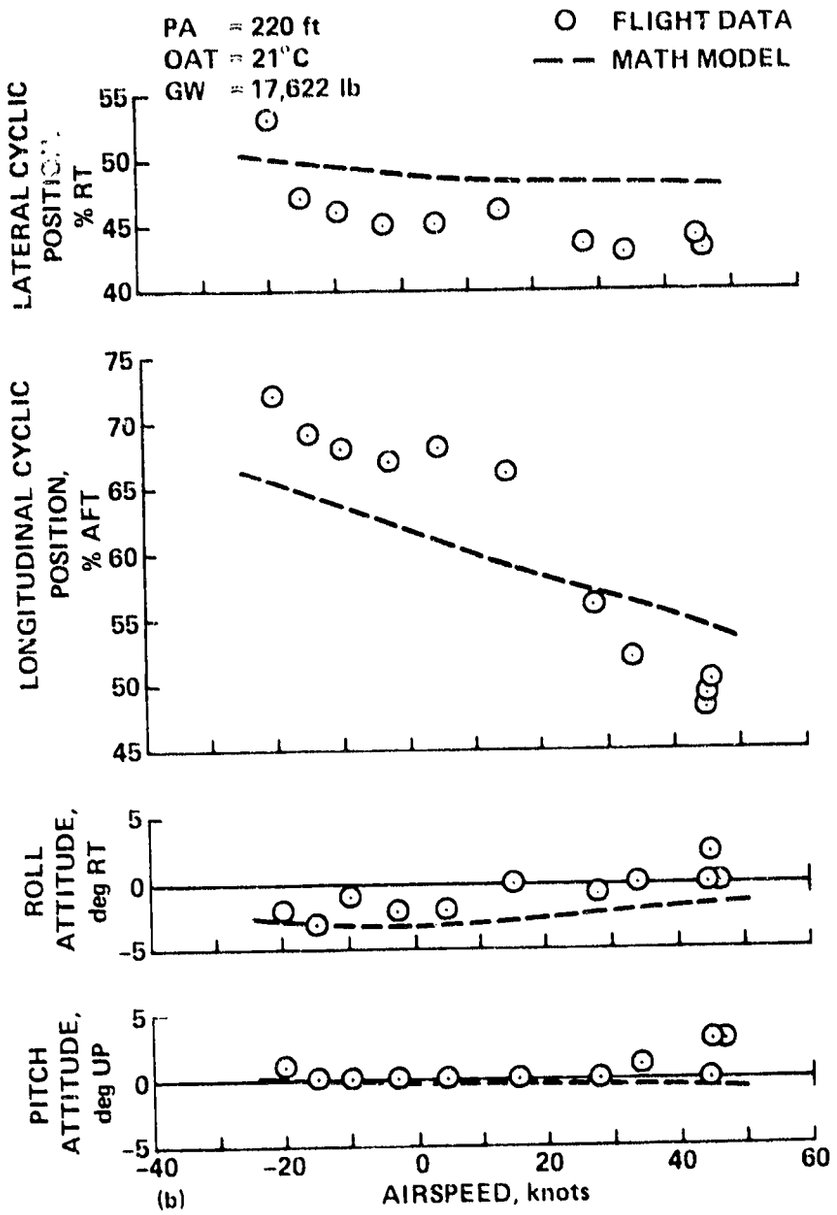

Figure 14.- Concluded.

Trimmed control positions versus sideslip are presented in figures 15(a) and (b). The math model pitch attitude and pedal position agree well with the flight-test data. The collective position and roll attitudes agree also for right sideslips and hover, but not left sideslips. The large negative roll angles of the math model are balanced by increases in the collective stick position, over the flight-test data. The large negative trim roll angles of the math model are probably due to inaccuracies in the fuselage rolling moment due to sideslip (figs. 15(a) and (b)).

The math model, longitudinal trimmed position shows the wrong trend though roughly the right magnitude. This can be explained by possible inaccuracies in the wind-tunnel data for pitching moment due to sideslip.

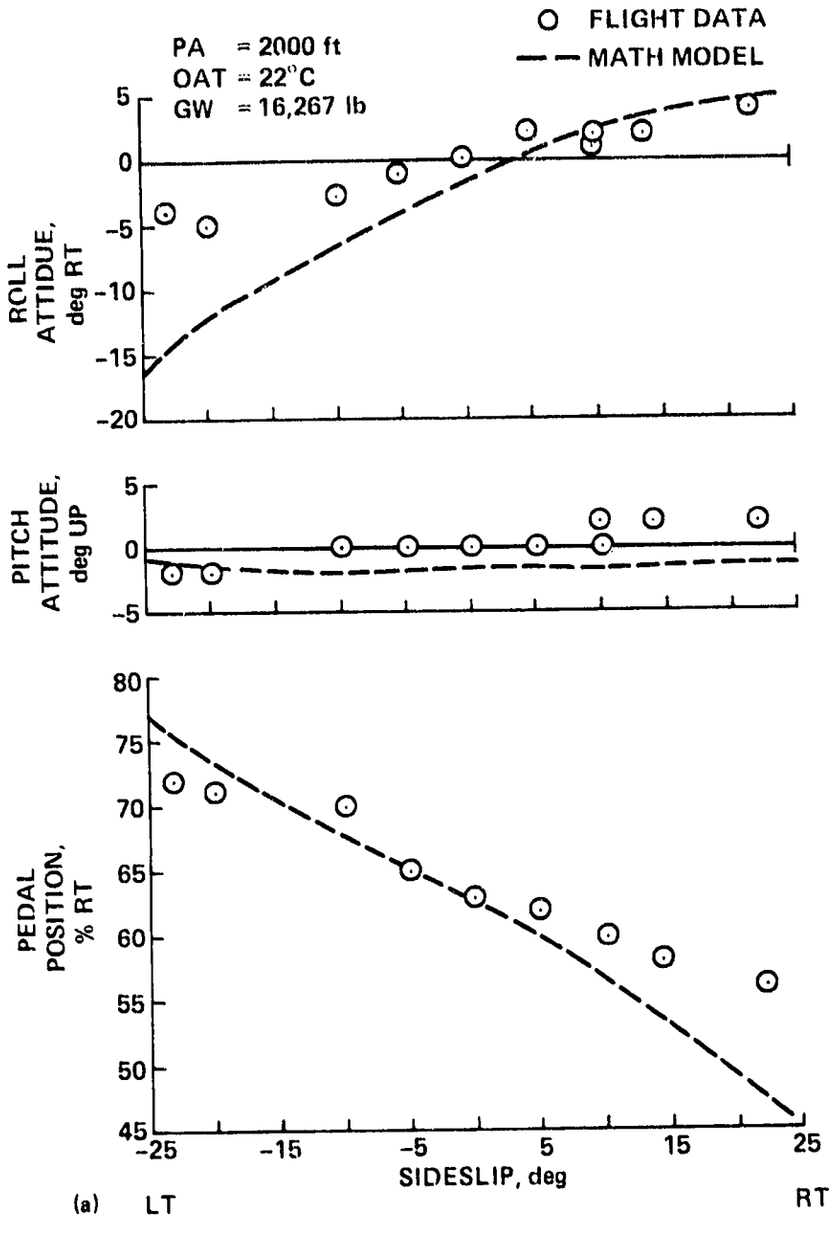

Figure 15.- Static lateral-directional stability.

Overall, the SH-3G math model agrees very well with flight data in performance and trimmed control positions throughout the airspeed range of the helicopter.

Dynamic Checks

The dynamic validation consists of a comparison with flight-test data for a 1 in. step in aft cyclic, a 1 in. step in right cyclic, a 1 in. step in right pedal, and a 20% torque increase (collective step) at a trim airspeed of 70 knots. Nominal flight conditions were 19,000-lb gross weight, 2,000 ft pressure altitude, and

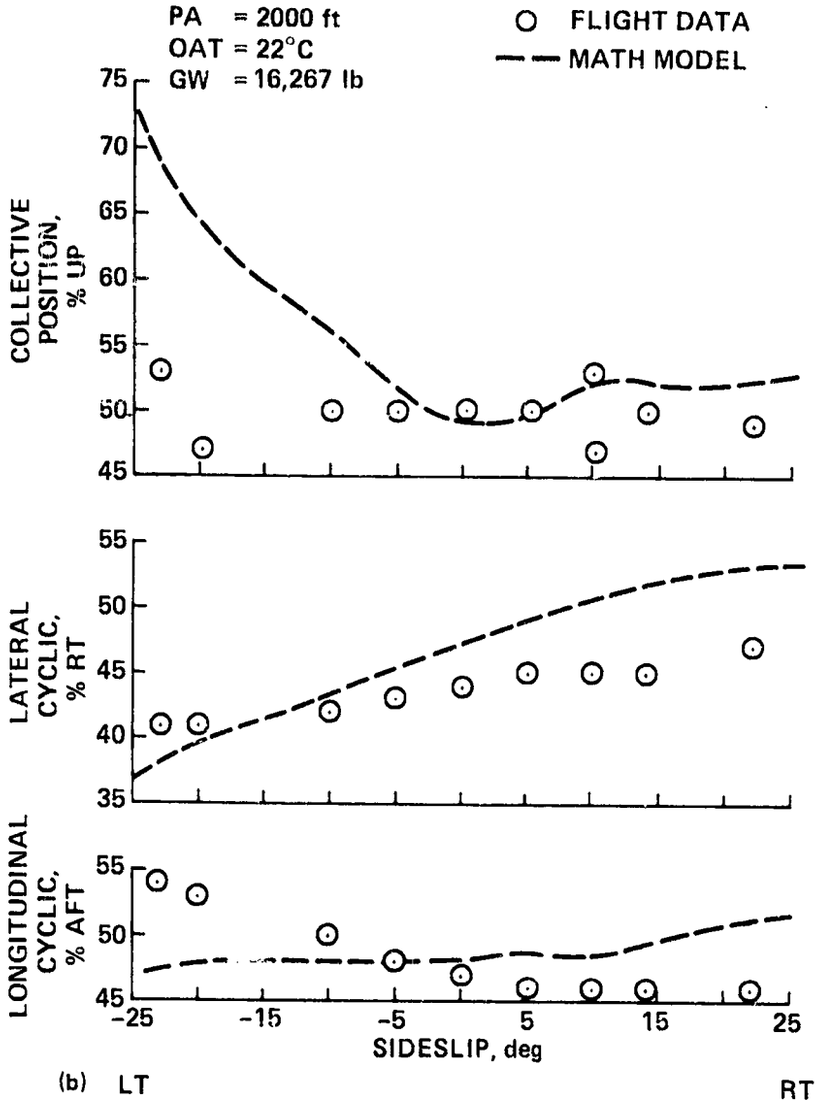

Figure 15.- Concluded.

standard temperature. In each case the pitch, roll, and yaw attitudes and pitch, roll, and yaw rates are examined. The results are presented in figures 16 to 19.

Figure 16 compares flight test data for a 1 in. aft cyclic step with the math model response for the same 1 in. cyclic step. Both the pitch rate and pitch attitudes are well modeled with approximately the right shape and amplitude. The roll and yaw parameters show the correct trend toward the end of the run and the math model is lightly coupled as is the actual helicopter.

A 1 in. right cyclic step is shown in figure 17. As can be seen, the shape in roll and roll attitude are correct and the magnitude of the roll attitude is approximately correct. The roll rate magnitude, however, is low for the math model by a factor of 2, reaching 20°/sec in the flight data and only 10°/sec for the math model. The effect of this can be seen in the roll response: the math model requires 3 sec to reach maximum attitude, while the flight data show only about 2 sec to reach

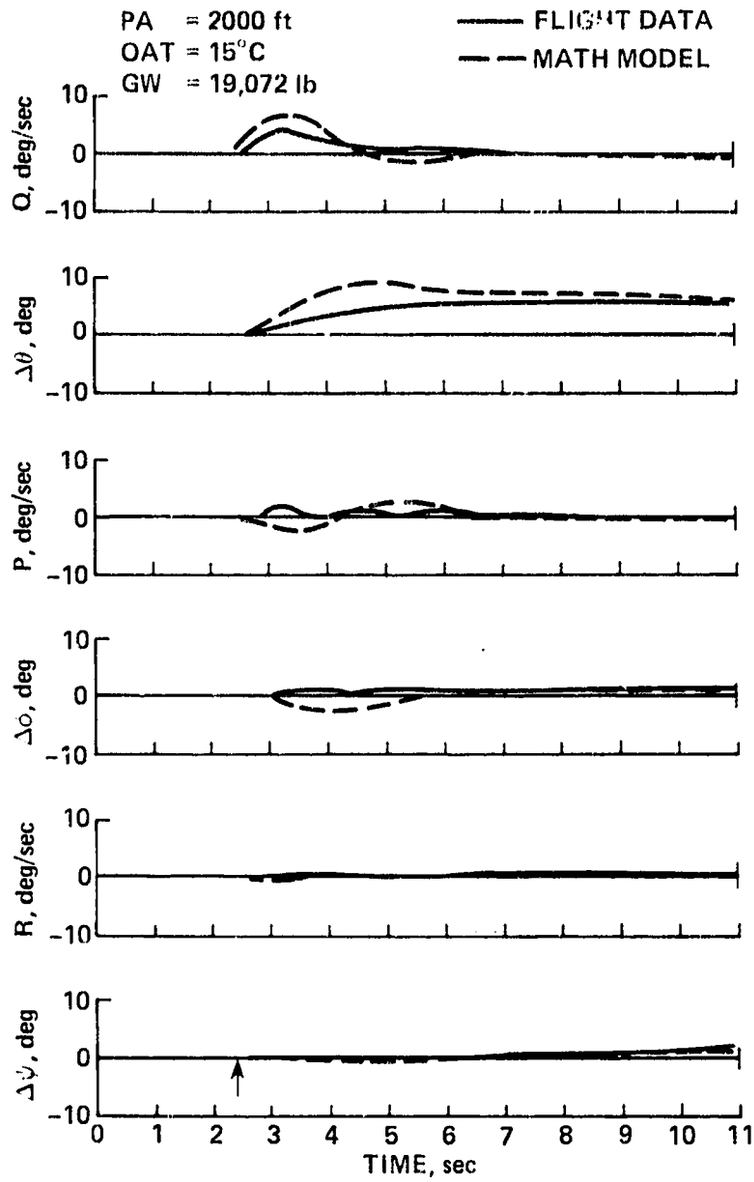

Figure 16.- One inch aft cyclic step.

maximum attitude change. This discrepancy remains unexplained, as the math model will not roll at 20°/sec with a 1 in. right cyclic step even with the control system off and only the main rotor natural damping operating.

The yaw attitude and yaw rate are well modeled showing the right shape and magnitude. The pitch attitude and rate is lightly coupled in both the math model and the flight data.

Figure 18 shows the response to a 1 in. right pedal step. The yaw rate and yaw attitude are very well modeled in shape and magnitude. The roll attitude is also well modeled in shape and magnitude. The math model roll rate is about double the flight-test data, reaching 7°/sec as opposed to 2°/sec in the flight data. The shape

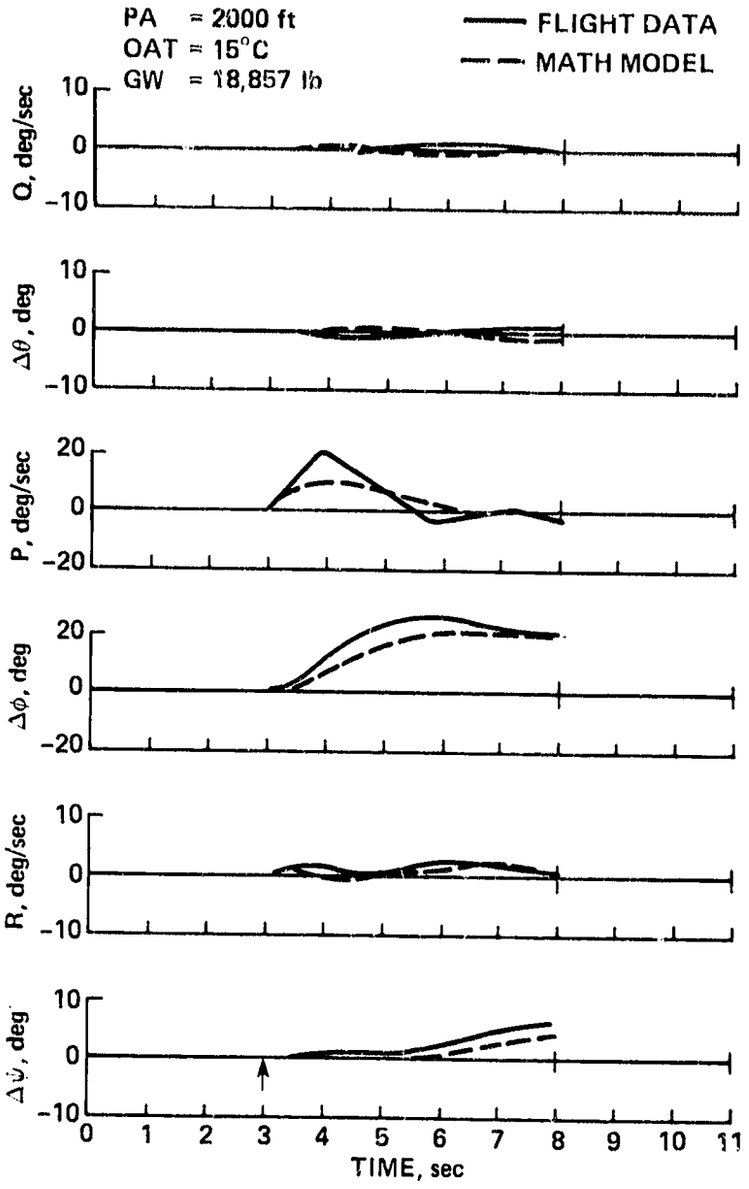

Figure 17.- One inch right cyclic step.

of the math modeled, roll-rate curve is correct, however. The pitch attitude and rate is very well modeled, although coupling is low.

A 20% torque increase or, effectively, a collective step is shown in figure 19. The yaw and yaw rate are particularly well modeled with similar frequency and amplitude between the flight data and math model. The roll rate and roll attitudes of the math model seem to be at a lower frequency and amplitude than the flight data. The pitch and pitch rate show roughly the same amplitude and shape for both the math model and flight-test data.

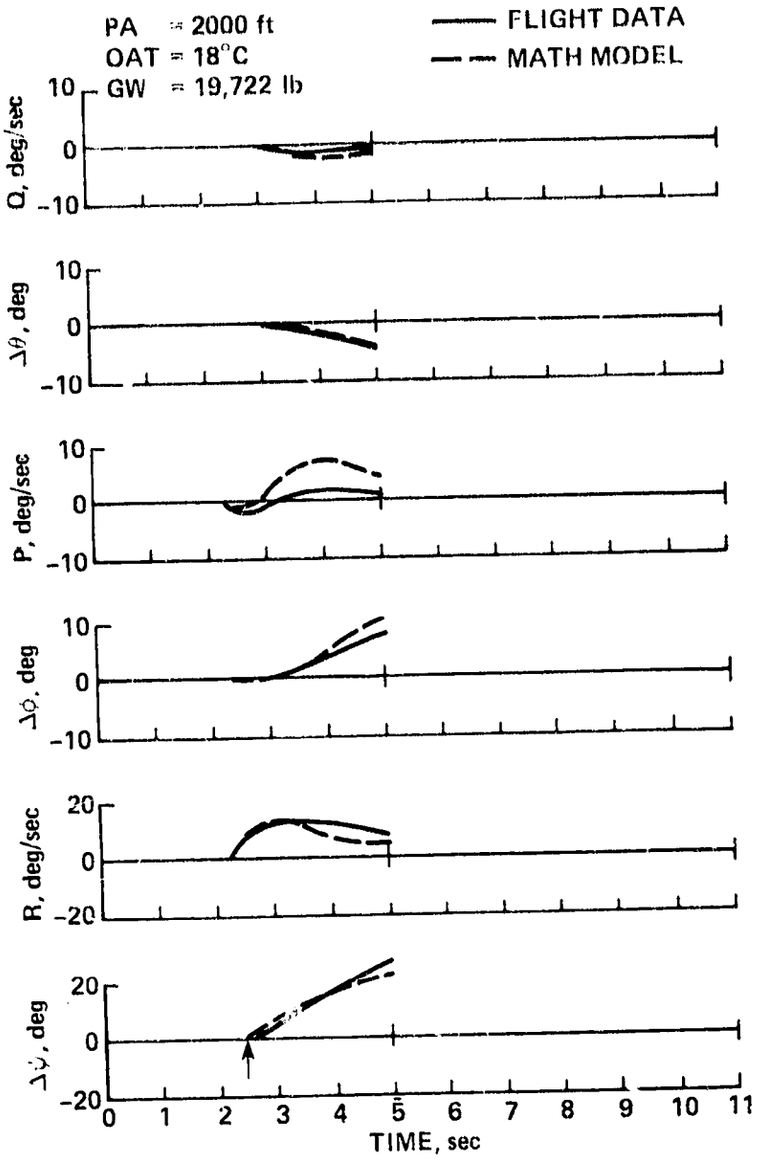

Figure 18.- One inch right pedal step.

Overall, the dynamic response in the primary axes, e.g., pitch response for longitudinal cyclic input, is modeled very well except for the roll rate. The coupled response is modeled fairly well and is small in any event.

CONCLUSIONS

A math model of the Sikorsky SH-3G helicopter well-matched to flight-test data and suitable for both off-line and real-time simulation has been developed at Ames Research Center. The model contains equations of motion, an atmospheric model, a

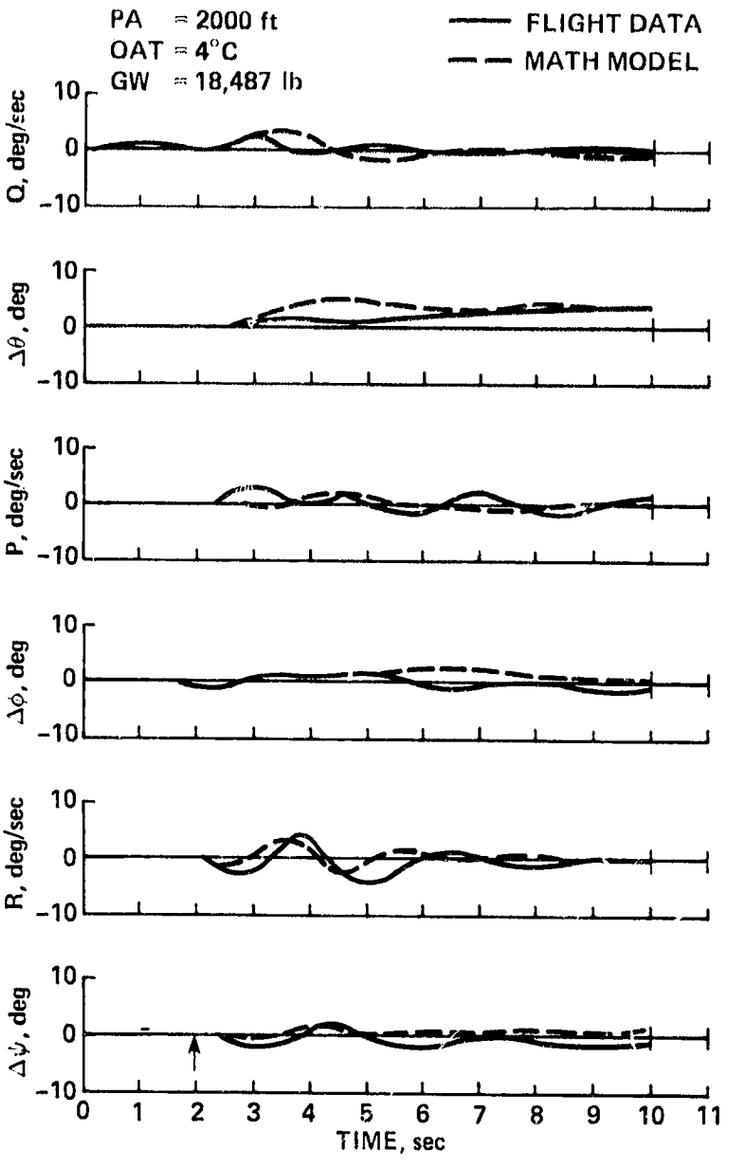

Figure 19.- 20% torque increase.

Dryden wind model, the fuselage aerodynamics, nonlinear main-rotor and tail-rotor models, a second-order engine model, and the SH-3G control system and rigging. An improved trim algorithm has also been developed.

1. The SH-3G math model performance and trimmed-control positions for airspeeds from -30 to 135 knots agree well in trend and magnitude with Navy flight-test data.

2. The math model dynamic response in attitude and rate to a 1 in. step in longitudinal cyclic, lateral cyclic, or pedals agrees fairly well in the primary axis with Navy flight-test data.

3. The following ad hoc procedure has improved the static trim accuracy of a simplified helicopter math model:

a. Reduce the blade lift curve slope until the trimmed collective position in hover matches flight data.

b. Increase the induced power term in the main rotor torque equation until engine torque in hover matches flight data.

c. Increase the fuselage flat-plate drag area until engine torque at 90 knots matches flight data.

APPENDIX A

VELOCITY INITIALIZATION

Three velocity vectors (air, wind, and inertial velocity) need to be initialized in two coordinate systems -- earth frame and body frame. This appendix contains a description of the various coordinate systems used, the problem, the solution, and some comments about special cases.

Earth axes relate to a triad of orthonormal vectors: $\hat{N}$, $\hat{E}$, $\hat{D}$, where $\hat{N}$ points north, $\hat{E}$ points east, and $\hat{D}$ points down into the earth. Body axes relate to another triad of orthonormal vectors $\hat{x}$, $\hat{y}$, $\hat{z}$, where $\hat{x}$ points out of the nose of an aircraft, $\hat{y}$ points out of the right wing, and $\hat{z}$ points down perpendicular to the plane of $\hat{x}$ and $\hat{y}$. A useful set of coordinates for this initialization problem is the $\hat{u}$, $\hat{m}$, $\hat{n}$ set or "path" coordinates; $\hat{u}$ points along the earth relative velocity, $\hat{m}$ is perpendicular to $\hat{u}$ and points right in the horizontal plane, and $\hat{n}$ points down perpendicular to the plane of $\hat{u}$ and $\hat{m}$. These coordinate systems are summarized by the three equations:

$$\bar{V}_e = V_N\hat{N} + V_E\hat{E} + V_D\hat{D} \quad \text{"earth" coordinates}$$

$$\bar{V}_b = V_x\hat{x} + V_y\hat{y} + V_z\hat{z} \quad \text{"body" coordinates}$$

$$\bar{V}_p = V_u\hat{u} + V_m\hat{m} + V_n\hat{n} \quad \text{"path" coordinates}$$

The trim initialization problem can be formally stated as follows:

Given:

V_a the air velocity magnitude

W_N wind component north

W_E wind component east

W_D wind component down

α angle of attack of the fuselage

β sideslip angle of the fuselage

γ_v vertical flightpath angle

γ_h horizontal flightpath angle

ϕ Euler roll angle

Find:

u_b x body axis component of the air velocity vector

V_b y body axis component of the air velocity vector

W_b z body axis component of the air velocity vector

V_N north component of the earth relative velocity vector

V_E east component of the earth relative velocity vector

V_D down component of the earth relative velocity vector

Va_N north component of the air velocity vector

Va_E east component of the air velocity vector

Va_D down component of the air velocity vector

θ Euler pitch angle

ψ Euler heading angle

Read the subscripts as follows:

a	air	h	horizontal
b	body	N	north
W	wind	E	east
v	vertical	D	down

The solution proceeds as follows:

From the definition of angle-of-attack and sideslip calculate the body axis components of airspeed.

$$u_b = V_a\, C\beta C\alpha$$

$$V_b = V_a\, S\beta$$

$$W_b = V_a\, C\beta S\alpha$$

From the definition of airspeed, wind, and ground speed:

$$\left.\begin{aligned} \bar{V} &= \bar{V}_a + \bar{W} \quad \text{or} \\ V\hat{u} &= V_a\hat{V}_a + W\hat{w} \end{aligned}\right\} \tag{A1}$$

Dot (A1) with $\hat{u}$, $\hat{m}$, and $\hat{n}$.

$$V = V_a(\hat{V}_a \cdot \hat{u}) + W(\hat{w} \cdot \hat{u}) = V_{a_u} + W_u \tag{A2a}$$

$$0 = V_a(\hat{V}_a \cdot \hat{m}) + W(\hat{w} \cdot \hat{m}) = V_{a_m} + W_m \tag{A2b}$$

$$0 = V_a(\hat{V}_a \cdot \hat{n}) + W(\hat{w} \cdot \hat{n}) = V_{a_n} + W_n \tag{A2c}$$

By definition:

$$V_a^2 = V_{a_u}^2 + V_{a_m}^2 + V_{a_n}^2 \tag{A3a}$$

$$W^2 = W_u^2 + W_m^2 + W_n^2 \tag{A3b}$$

Rewriting (A2b) and (A2c):

$$V_{a_m} = -W_m \tag{A2b}$$

$$V_{a_n} = -W_n \tag{A2c}$$

Substituting (A2b) and (A2c) into (A3a):

$$V_a^2 = V_{a_u}^2 + W_m^2 + W_n^2 \tag{A4}$$

Solving (A3b) for $(W_m^2 + W_n^2)$ and substituting into (A4):

$$V_{a_u}^2 = V_a^2 - (W^2 - W_u^2)$$

Substituting into (A2a):

$$V = \sqrt{V_a^2 - (W^2 - W_u^2)} + W_u \tag{A5}$$

Transforming a vector from earth coordinates to path coordinates requires two pure rotations.

$$\bar{W}_p = T_{\gamma_v} T_{\gamma_h} \bar{W}_e$$

where

$$T_{\gamma_v} = \begin{vmatrix} C\gamma_v & 0 & -S\gamma_v \\ 0 & 1 & 0 \\ S\gamma_v & 0 & C\gamma_v \end{vmatrix}, \quad T_{\gamma_h} = \begin{vmatrix} C\gamma_h & S\gamma_h & 0 \\ -S\gamma_h & C\gamma_h & 0 \\ 0 & 0 & 1 \end{vmatrix}$$

Applying the above transformation:

$$\begin{pmatrix} W_u \\ W_m \\ W_n \end{pmatrix} = \begin{vmatrix} C\gamma_v C\gamma_h & C\gamma_v S\gamma_h & -S\gamma_v \\ -S\gamma_h & C\gamma_h & 0 \\ S\gamma_v C\gamma_h & S\gamma_v S\gamma_h & C\gamma_v \end{vmatrix} \begin{pmatrix} W_N \\ W_E \\ W_D \end{pmatrix}$$

And the component of the wind parallel to the earth relative velocity vector is:

$$W_u = C\gamma_v C\gamma_h \cdot W_N + C\gamma_v S\gamma_h \cdot W_E - S\gamma_v \cdot W_D \tag{A6}$$

With the earth relative velocity magnitude from equation (A5) and the definition of γ_v and γ_h:

$$V_N = V\, C\gamma_v C\gamma_h$$

$$V_E = V\, C\gamma_v S\gamma_h$$

$$V_D = V(-S\gamma_v)$$

Equation (A1) now gives:

$$\begin{pmatrix} Va_N \\ Va_E \\ Va_D \end{pmatrix} = \begin{pmatrix} V_N \\ V_E \\ V_D \end{pmatrix} - \begin{pmatrix} W_N \\ W_E \\ W_D \end{pmatrix}$$

From the definition of body axes:

$$\begin{pmatrix} U_b \\ V_b \\ W_b \end{pmatrix} = T_\phi T_\theta T_\psi \begin{pmatrix} Va_N \\ Va_E \\ Va_D \end{pmatrix}$$

where θ and ψ are still unknown and T_ϕ, T_θ, and T_ψ are defined in equation (1) of the main text.

Separating θ and ψ:

$$T_\theta^{-1} T_\phi^{-1} \begin{pmatrix} U_b \\ V_b \\ W_b \end{pmatrix} = T_\psi \begin{pmatrix} Va_N \\ Va_E \\ Va_D \end{pmatrix}$$

Multiplying out:

$$\begin{pmatrix} C\theta & 0 & S\theta \\ 0 & 1 & 0 \\ -S\theta & 0 & C\theta \end{pmatrix} \begin{pmatrix} U_b \\ V_b C\phi - W_b S\phi \\ V_b S\phi + W_b C\phi \end{pmatrix} = \begin{vmatrix} C\psi & S\psi & 0 \\ -S\psi & C\psi & 0 \\ 0 & 0 & 1 \end{vmatrix} \begin{pmatrix} Va_N \\ Va_E \\ Va_D \end{pmatrix} \qquad \text{(A7a)}$$

$$\text{(A7b)}$$

$$\text{(A7c)}$$

Note that (A7b) is independent of θ and (A7c) is independent of ψ:

$$V_b\, C\phi - W_b\, S\phi = -Va_N\, S\psi + Va_E\, C\psi \qquad \text{(A7b)}$$

$$-U_b\, S\theta + (V_b\, S\phi + W_b\, C\phi)C\theta = Va_D \qquad \text{(A7c)}$$

Equations (A7b) and (A7c) can now be put in the form:

$$A \sin(q) = B \cos(q) + C \tag{A8}$$

This can be solved for q as follows:

$$\sqrt{A^2 + B^2}\left[\frac{A}{\sqrt{A^2 + B^2}}\sin(q) - \frac{B}{\sqrt{A^2 + B^2}}\cos(q)\right] = C$$

or

$$\cos(r)\sin(q) - \sin(r)\cos(q) = \frac{C}{\sqrt{A^2 + B^2}}$$

where $\tan(r) = B/A$; then $\sin(q - r) = C/\sqrt{A^2 + B^2}$. Solving for q and substituting for r:

$$q = \arctan\left(\frac{B}{A}\right) + \arcsin\left(\frac{C}{\sqrt{A^2 + B^2}}\right) \tag{A9}$$

Rewriting (A7b) in the form of (A8):

$$V_{a_N} S\psi = V_{a_E} C\psi + (W_b S\phi - V_b C\phi) \tag{A7b}$$

Applying (A9):

$$\psi = \arctan\left(\frac{V_{a_E}}{V_{a_N}}\right) + \arcsin\left(\frac{W_b S\phi - V_b C\phi}{V_{a_g}}\right) \tag{A10}$$

where

$$V_{a_g} = \sqrt{V_{a_N}^2 + V_{a_E}^2}\ ; \quad V_{a_N} \neq 0 \quad \text{and} \quad V_{a_g} > 0$$

Rewriting (A7c) in the form of (A8):

$$U_b S\theta = (V_b S\phi + W_b C\phi)C\theta - V_{a_D} \tag{A7c}$$

Applying (A9):

$$\theta = \arctan\left(\frac{V_b S\phi + W_b C\phi}{U_b}\right) + \arcsin\left[\frac{-V_{a_D}}{\sqrt{U_b^2 + (V_b S\phi + W_b C\phi)^2}}\right] \tag{A11}$$

where $U_b \neq 0$ and $V_a \neq 0$.

Note that for $\phi = \psi = 0$:

$$\gamma = \arctan\left(\frac{V_{a_E}}{V_{a_N}}\right) = \gamma_h$$

and:

$$0 = \arcsin\left(\frac{-V_{a_D}}{\sqrt{U_b^2 + W_b^2}}\right) + \arctan\left(\frac{W_b}{U_b}\right) = \gamma_v + \alpha$$

as required. Rearward flight is handled by adding 180° to β and γ_v. This implies α and γ_h should be limited to ±90°. This limitation results from the definitions:

$$\bar{V}_a = T_\beta T_\alpha \bar{V}_b$$

$$\bar{V}_p = T_{\gamma_v} T_{\gamma_h} \bar{V}_e$$

In words, the air-velocity direction is defined by two rotations (α and β) from body axes and the path-velocity vector is defined by two rotations (γ_h and γ_v) from earth axes. To rotate the velocity vector to the opposite direction, the last rotation angle (β or γ_v) must be used, instead of α or γ_h, or the resulting vector will not, in general, point in the opposite direction.

Hover is handled by not allowing the total air velocity to equal zero exactly. If the air-velocity magnitude is less than some small criterion, then the air velocity is assigned the criterion value times the sign of the velocity. Mathematically:

$$\text{If} \quad |V_a| < V_\varepsilon \,, \quad \text{then} \quad V_a = \text{sign}(V_a) \times V_\varepsilon$$

The method described in this appendix is valuable for solving other similar problems. Particularly useful are the two "tricks" embodied in equations (A5) and (A9).

APPENDIX B

SYMBOLS

A_{1_s}, B_{1_s}	lateral and longitudinal cyclic control angles in shaft axes
ASE_c	collective channel automatic-control command
ASE_{la}	lateral channel automatic-control command
ASE_{lo}	longitudinal channel automatic-control command
ASE_t	yaw channel automatic-control command
a	blade lift curve slope, rad
a'	angle of tilting of the thrust vector due to lift
a_0	rotor coning angle
a_{0t}	tail rotor blade coning angle
a_1, b_1	lateral and longitudinal flapping angles in control axes
a_{1_s}, b_{1_s}	lateral and longitudinal flapping angles in shaft axes
B	blade tip loss factor
b	number of blades
$C_1 \ldots C_{10}$	moment of inertia coefficients (eq. (12))
$C_{F_{D_0}}$	fuselate flat-plate drag area
$C_{F_{D_1}}$	fuselage drag-force coefficient due to local angle of attack
$C_{F_{D_2}}$	fuselage drag-force coefficient due to local sideslip
$C_{F_{L_1}}$	fuselage lift-force coefficient due to local angle of attack
$C_{F_{L_2}}$	fuselage lift-force coefficient due to sideslip
C_{F_y}	fuselage side-force coefficient
C_{M_ℓ}	rolling-moment coefficient
$C_{M_{m_1}}$	pitching-moment coefficient due to local angle of attack
$C_{M_{m_2}}$	pitching-moment coefficient due to sideslip
C_{M_n}	yawing-moment coefficient
C_q	torque coefficient, $Q/\rho(\Omega R)^2 \pi R^5$

C_{T_m}	main rotor-thrust coefficient
C_y	rotor side-force coefficient
c	rotor blade chord
D	fuselage drag force, (+ aft)
DT	computer cycle time or integration step
e	rotor flapping-hinge offset
e_{kf}	fuselage angle-of-attack correction for main rotor downwash
e_m	main rotor downwash factor
Fa_x, Fa_y, Fa_z	fuselage aerodynamic force components
F_G	gravitational force
F_N, F_E, F_D	force in earth axes
F_x, F_y, F_z	force in body axes
Fx_s, Fy_s, Fz_s	force in shaft axes
G	gradient gain on the Jacobian matrix
G_R	control gain on yaw rate
G_{bah}	control gain on altitude error
G_c	control gain on collective stick position
G_p	control gain on roll rate
G_r	gear ratio between the main and tail rotors, 6.28937
$G_{x_{1a}}$	control gain on lateral cyclic-stick position
$G_{x_{1o}}$	control gain on longitudinal cyclic-stick position
G_θ	control gain on pitch angle
G_ϕ	control gain on bank angle
G_ψ	control gain on heading error
H	rotor drag force
h	altitude above sea level
h_{ref}	control reference altitude, set when the altitude hold switch is turned on

I	effective inertia of the main rotor, I_m
I_m	moment of inertia of the main rotor blades and hub
I_{xx}, I_{yy}, I_{zz}	body axis moments of inertia
J	rotor side force
K_c	rigging constant between collective stick and collective pitch
K_{c-la}	coupling between collective stick and lateral swashplate angle
K_{c-lo}	coupling between collective stick and longitudinal swashplate angle
K_{c-t}	coupling between collective stick and tail-rotor pitch
K_d	engine governor constant affecting the derivative of Δrpm in the characteristic equation
K_i	engine governor gain on the time integral of rpm error
K_{la}	rigging constant between lateral cyclic stick and lateral cyclic-control angle
K_{lo}	rigging constant between longitudinal cyclic stick and longitudinal cyclic-control angle
K_{sw}	thrust correction for rotor spanwise flow not accurately modeled
K_{nu}	thrust correction for nonuniform flow
K_t	rigging constant between pedal position and tail-rotor collective
L, M, N	rolling, pitching, and yawing moments in body axes
L_0	magnitude of a generalized step load on the engine
LAT	latitude of the helicopter
LON	longitude of the helicopter
L_f	fuselage lift force (+ up)
L_s, M_s, N_s	pure rolling, pitching, and yawing moments in shaft axes
M	Mach number
m	mass of the helicopter
m_w	mass moment of a rotor blade
n	count of current time step
P, Q, R	body axes roll, pitch, and yaw rates
P, T	free-stream temperature and pressure

P_c, Q_c, R_c	control axes roll, pitch, and yaw rates
P_s, Q_s, R_s	shaft axes roll, pitch, and yaw rates
Q_e	engine torque
Q_m	main-rotor torque
Q_t	tail-rotor torque
q	dynamic pressure
q_c	compressible dynamic pressure, as measured by a pitot static tube
R	rotor disc radius
R_e	radius of the earth, 20,898,908 ft
S_{ase}	automatic stabilization equipment switch (1 = On)
S_{bah}	barometric altitude hold switch (1 = On)
s	Laplace transform variable
T	rotor thrust
Ta_ℓ, Ta_m, Ta_n	fuselage aerodynamic moments in body axes
Ta_r, Pa_r	ratio of standard temperature and pressure at altitude to sea-level values
T_r, T_r	total temperature and pressure ratios
T_{tot}, P_{tot}	total temperature and pressure
U_b, V_b, W_b	airspeed in body axes
U_c, V_c, W_c	airspeed in control axes
U_s, V_s, W_s	airspeed in shaft axes
V	earth relative velocity magnitude
V_a	airspeed magnitude
V_{a_g}	ground speed
Va_N, Va_E, Va_D	airspeed in earth axes
Va_u, Va_m, Va_n	airspeed in path axes
V_{cal}	calibrated airspeed corrected for the effects of compressibility
V_{eq}	equivalent airspeed at sea-level density

V_N, V_E, V_D	earth relative velocity in earth axes
W_N, W_E, W_D	wind velocity in earth axes
W_u, W_m, W_n	wind velocity in path axes
X_c	collective stick position
x_h, y_h, z_h	coordinates of the rotor hub relative to the CG in body axes
X_{1a}	lateral cyclic-stick position
X_{1o}	longitudinal cyclic-stick position
X_t	tail rotor pedal position
Y	fuselage side force (+ right)
Z_1, Z_2, Z_3	rotor constants defined by equation (61)
α	fuselage centerline angle of attack
α_ℓ	fuselage centerline angle of attack corrected for main rotor downwash
α_r	average rotor-blade angle of attack in hover
β	sideslip angle of fuselage (+ nose left of velocity vector)
β_r	rotor orientation angle
γ	rotor lock number
γ_h	horizontal flightpath angle (eq. (5))
γ_v	vertical flightpath angle (eq. (5))
ΔRPM	main-rotor rpm deviation from nominal (203.3)
ΔT	temperature above standard conditions
δ	rotor-blade profile-drag coefficient
$\delta_0, \delta_1, \delta_2$	coefficients of the Bailey profile-drag coefficient (eq. (49))
δ_3	tail-rotor δ_3 hinge phase angle
θ_0	rotor collective pitch angle
θ_{0t}	tail rotor collective pitch angle
$\theta_{0,0}$	lowest main-rotor collective pitch
$\theta_{0t,0}$	neutral tail-rotor collective pitch with collective in full low position
θ_1	rotor blade twist from root to tip

θ_{75}	blade pitch at 75% of the rotor-disc radius
θ_{ct}	tail-rotor commanded collective pitch
λ_m	main-rotor inflow ratio
μ_m	main-rotor tip-speed ratio
ν	induced inflow ratio
ρ	atmospheric density
σ	rotor solidity ratio
τ_{1a}	lateral channel filter-time constant
τ_t	yaw channel filter-time constant
$\tau_{x_{1a}}$	lateral stick filter-time constant
$\tau_{x_{1o}}$	longitudinal stick filter-time constant
τ_ν	lag time constant for changes in the inflow ratio
ϕ,θ,ψ	roll, pitch, and yaw Euler angles
ϕ_s,θ_s	rotor-shaft roll and pitch relative to the (-Z) body axis
ψ_0	rotor flapping phase angle
ψ_{ref}	reference heading
Ω	main rotor angular rate
ω_e	angular rate of the earth, 0.000072722 rad/sec

Vectors

$\hat{N},\hat{E},\hat{D}$	unit vectors along earth axes
$\hat{u},\hat{m},\hat{n}$	unit vectors along path axes
$\hat{x},\hat{y},\hat{z}$	unit vectors along body axes
x,u	state and control vectors for trimming
ε	trim-error criteria for stopping the trim process

Matrices

J	Jacobian matrix-matrix of partial derivatives
T_β,T_α	rotation matrices for locating the airspeed vector relative to body axes

$T_{\gamma_v}, T_{\gamma_h}$	rotation matrices for locating the earth relative vector on the earth
T_ϕ, T_θ, T_ψ	rotation matrices for converting earth axes to body axes

Subscripts

b	body axes
c	control axes (aligned to the axis of no feathering)
e	earth axes
m	main rotor parameters
p	path coordinates (see appendix A)
s	shaft axes (aligned to the rotor shaft axis)
t	tail-rotor parameters
$(\dot{})$	time derivative

REFERENCES

1. Schaughnessy, J. D.; Deau, Thomas N.; and Yenni, Kenneth R.: The Development and Validation of a Piloted Simulation of a Helicopter and External Sling Load. NASA TP-1285, 1979.

2. Bailey, F. J., Jr.: A Simplified Theoretical Method of Determining the Characteristics of a Lifting Rotor in Forward Flight. NACA Report 716, 1941.

3. Bramwell, A. R. S.: Helicopter Dynamics. Edward Arnold Ltd. (London), 1976.

4. Sturgeon, W. R.; and Phillips, J. D.: A Mathematical Model of the CH-53 Helicopter. NASA TM-81238, 1980.

5. O'Connell, Lt. J. T., Jr.; and Edris, Mr. J. H.: SH-3H Helicopter Criteria for the Device 2F64C Trainer. First Interim Report. Report RW-38R-78, Department of the Navy, Naval Air Test Center, 1979. (Available from Commander, Naval Air Test Center, Patuxent River, Maryland 20670).

6. McFarland, R. E.: A Standard Kinematic Model for Flight Simulation at NASA_Ames. NASA CR-2497, 1975.

7. Neuman, Frank; and Foster, J. D.: Investigation of a Digital Automatic Aircraft Landing System in Turbulence. NASA TN D-6066, 1970.

8. Trainer Math Model Report: SH-3H Helicopter Operational Flight Trainer Device 2F64C, Contract N61339-74-0103-0006; Data Item A002, Reflectone Report 808-A002, Reflectone, Inc., 1975.

9. Monteleone, R. A.: A Research and Development Program Performed to Develop Pilot Technique and Design Criteria to Increase Safety in the Event of Tail Rotor System Malfunction, SER-50384, Volume 1, 1964. (Available from Chief, Bureau of Naval Weapons, Washington 25, D.C.)

10. Jacobs, E. N.; and Sherman, Albert: Airfoil Section Characteristics as Affected by Variations of the Reynolds Number. NACA Report 586, 1937.

11. NATOPS Flight Manual SH-3G,HH-3A,UH-3A Helicopters, NAVAIR 01-230HLC-1, 1980.

12. Phelan, R. M.: Automatic Control Systems. Cornell University Press, 1977.

13. Handbook Maintenance Instructions Navy Models SH-3A, SH-3G, and HH-3A Helicopters Airframe Group. NAVAIR 01-230HLC-2-2, 1976.

14. Talbot, Peter D.; Tinling, Bruce E.; Decker, William A.; and Chen, Robert T.: A Mathematical Model of a Single Main Rotor Helicopter for Piloted Simulation. NASA TM-84281, September 1982.

15. McFarland, R. E.: BQUIET A Six-Degrees-of-Freedom Trim Process Fully Integrated into the BASIC System. NASO 72-12, 1972.